RESEARCH ACTIVITIES VI
Department of Vacuum UV Photoscience

VI-A Electronic Structure and Decay Mechanism of Inner-Shell Excited Molecules

This project is being carried out at the Beamline 4B of the UVSOR facility and at the surface station of the Beamline I-511 of the MAX-II facility in collaboration with the Uppsala University. Dr. Takaki Hatsui has been working as a research associate since August 2000, and Dr. Mitsuru Nagasono as a JSPS postdoctoral fellow since April 2000. We are interested in linear polarization dependence of inner-shell resonant excitations for simple molecules. We have two subprojects: (A) spin-orbit, exchange, and molecular field splittings in S 2p and P 2p excited states and (B) molecules and radicals in condensed phase and in rare gas matrix. In the subproject (A) we are happy to report here a hot result obtained by using a newly-constructed BL4B of UVSOR. In the subproject (B) we have constructed a new apparatus as shown Figure 1. For both the subprojects theoretical investigation is essential and some theoretical approaches are now under development.

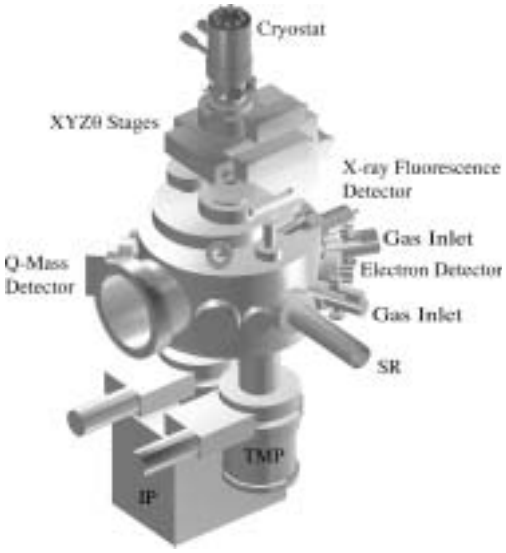

Figure 1. A new apparatus to investigate molecules and radicals in condensed phase and in rare gas matrix.

VI-A-1 Spin-Orbit and Exchange Splittings in the S 2p $\rightarrow \pi^*(b_1)$ Excitation of SO_2

KOSUGI, Nobuhiro; HATSUI, Takaki; NAGASONO, Mitsuru; GEJO, Tatsuo; SHIGEMASA, Eiji

Figure 1 shows a part of angle-resolved photoion yield spectra (ARPIS) of SO_2, where I_0 (I_{90}) corresponds to ion yields in the direction parallel (perpendicular) to the electric vector of the linear polarized incident light. The photon energy region shown is very narrow, only 3 eV from 164 eV to 167 eV. This region includes only the S 2p excitation to the lowest unoccupied orbital of $\pi^*(b_1)$ symmetry. The S 2p orbitals have a_1, b_2 and b_1 symmetries, resulting in three S 2p-π^* (b_1) excited states of B_1, A_2, and A_1 symmetries. The ground state symmetry is A_1 and the $A_2 \leftarrow A_1$ excitation is dipole-forbidden; that is, the $a_1 \rightarrow b_1^*$ (B_1) and $b_1 \rightarrow b_1^*$ (A_1) excitations should be observed in Figure 1. Considering the spin-orbit interaction, each singlet excitation is mixed with two triplet excitations, resulting in three dipole-allowed excited states in each symmetry. The transition dipoles to the B_1 states are orthogonal to the molecular plane and these transitions give only I_{90} yields; on the other hand, the transitions to the A_1 states give both I_0 and I_{90} yields. In Figure 1, three electronic states of B_1 symmetry show vibrational fine structures, where the lowest electronic state is very weak, and the second ($^2P_{3/2}$) is stronger than the third ($^2P_{1/2}$). On the other hand, Figure 1 shows only two electronic states of A_1 symmetry, where one is located in the $^2P_{3/2}$ manifold, and the other is in the $^2P_{1/2}$ manifold. The $^2P_{1/2}$ feature seems to be slightly stronger that the $^2P_{3/2}$ feature, though the $^2P_{3/2}$ branch is as twice large as the $^2P_{1/2}$ branch in the case of ionization. This indicates that exchange interaction is essential in the A_1 symmetry. This is reasonable, considering that the $2pb_1$ and π^*b_1 orbitals are oriented parallel. Furthermore, the singlet excited state is quite higher in energy than the triplet excited state, and the lowest state of A_1 symmetry hardly borrows intensity from the singlet component; therefore, the lowest state is invisible in the spectra as shown in Figure 1.

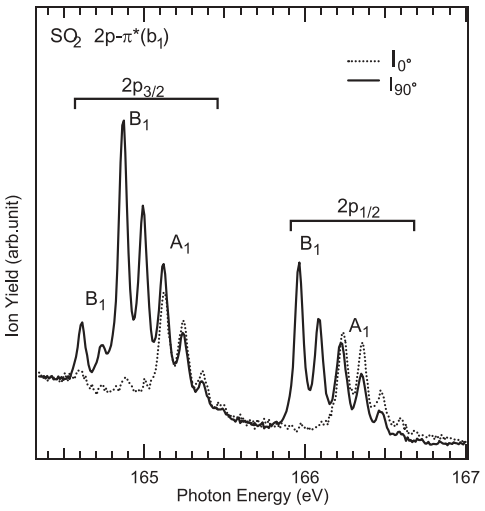

Figure 1. High resolution ARPIS of the spin-orbit split transitions to the S $2pa_1 \rightarrow \pi^*b_1$ (B_1) and S $2pb_1 \rightarrow \pi^*b_1$ (A_1) excited states of SO_2.

VI-A-2 X-Ray Photoelectron and Absorption Spectra of Fragments from NH_3/Cu(110) Induced by Soft X-Ray Irradiation

NAGASONO, Mitsuru; NORDLUND, Dennis[1,2]; NILSSON, Anders[2]; KOSUGI, Nobuhiro
([1]Max-lab; [2]Uppsala Univ.)

We have studied fragments from NH_3 adsorbed on Cu(110) using N 1s x-ray photoelectron spectroscopy and x-ray absorption spectroscopy in combination with theoretical calculations. As shown in Figure 1, three N1s photoemission peaks arising under soft x-ray irradiation are assigned to NH_x (x = 0, 1, and 2) species on Cu(110). These peaks are enhanced in sequence of x = 2, 1, and 0; *i.e.*, at first the NH_2 species are produced from the NH_3, the NH from the NH_2, and the N from the NH. These fragments are produced by Auger stimulated dissociation (ASD) process and/or x-ray-induced electron-stimulated dissociation (XESD). In the ASD process, fragmentation of NH_3 leads to all NH_x species simultaneously. While in the XESD process, the fragmentation leads to only NH_2 species from NH_3. Therefore the XESD is a dominant process, but the ASD is a minor one. The fragments produced at the early stage correspond to NH_2 anions by considering theoretical predictions. This result suggests a charge transfer process from the Cu substrate to the adsorbed NH_2 radical prepared following the XESD process.

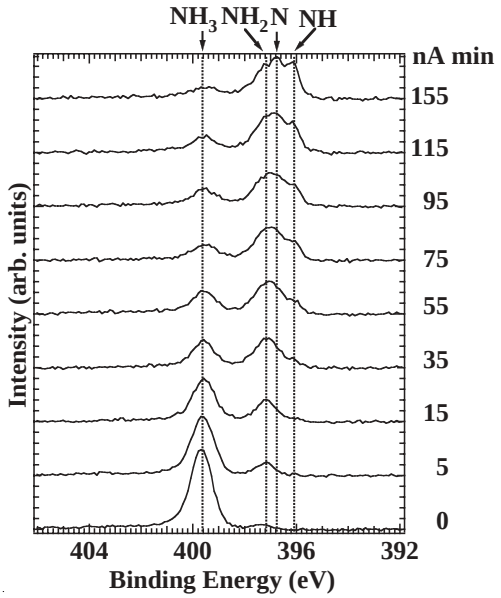

Figure 1. N 1s XP spectra of NH_3/Cu(110) as a function of exposure to x-ray.

VI-B Soft X-ray Photoelectron-Photoabsorption Spectroscopy and Electronic Structure of Transition Metal Compounds

This project is being carried out by the Kosugi group at the Beamline 1A of the UVSOR facility and at the bulk station of the Beamline I-511 of the MAX-II facility in collaboration with the Uppsala University. Dr. Hiroshi Oji has been working as a postdoctoral IMS fellow since April 2000, and Dr. Takaki Hatsui as a research associate since August 2000. We are interested in linear polarization dependence of inner-shell resonant excitations (UVSOR) for planar complex molecules/ions in the single crystal, and in resonantly-emitted photoelectron (UVSOR) and photon (MAX-II) spectroscopies for the same systems by tuning the photon energy to inner-shell resonances. In the UVSOR facility we are using crystal monochromators, which restrict the photon energy to the range higher than the Cu and Ni 2p edge (> 800 eV). Recently, we have decided to move our experimental apparatus to the BL 4B, which is a new beamline covering the lower photon energy (< 800 eV). Next year we hope we will show new results on some interesting materials containing Fe, Mn, and so on.

VI-B-1 Photoabsorption and Resonant Photoelectron Spectroscopy of a Rare-earth Borocarbide LaB_2C_2

OJI, Hiroshi; HASEGAWA, Shinji; SUZUKI, Kazuya; KOSUGI, Nobuhiro

Rare-earth borocarbides RB_2C_2 (R: rare-earth (RE) metals) are intercalation compounds in which rare-earth metal cations are intercalated in the planar BC sheets. These compounds show interesting electronic and magnetic properties, such as superconducting behavior (T_c = 2.4 K for LuB_2C_2[1)]). Therefore it is important to know their electronic structure in order to clarify the mechanism of these properties. In this study, the La 3d photoabsorption (hν ~ 830 eV) and resonant valence-band photoelectron spectra of lanthanum borocarbide (LaB_2C_2) were measured to reveal the partial density of states at the core-excited atom is enhanced in resonant photoelectron spectra. Use of the relatively high energy photons of BL1A at UVSOR facility allows us to perform the bulk-sensitive measurements. The off- (hν = 826.4 eV) and on- (834.3 eV) resonant photoelectron spectra of LaB_2C_2 in the valence region are shown in

Figure 1. Abscissa represents the binding energy relative to the Fermi level (E_F). La 3d-4f photoabsorption spectrum of LaB_2C_2 is also indicated in the inset. A La 5p band (~20 eV) and some bands near to the E_F (0–7 eV) are significantly enhanced in the on-resonant spectrum. The latter resonant enhancement suggests that some valence states near to E_F are localized on La atom. This does not support the complete donation of the three valence electrons of La to the BC sheet, but means that some valence electrons (according to the theoretical band calculation,[2] La 5d-derived electrons) of La atom are participating to the formation of the valence band of LaB_2C_2. The number of La 5d derived-valence electron localized on a La atom is roughly estimated to be 0.3.

References

1) J. van Duijn *et al.*, *Phys. Rev. B* **62**, 6410 (2000).
2) H. Harima and M. Shirai, *J. Phys. Soc.* submitted.

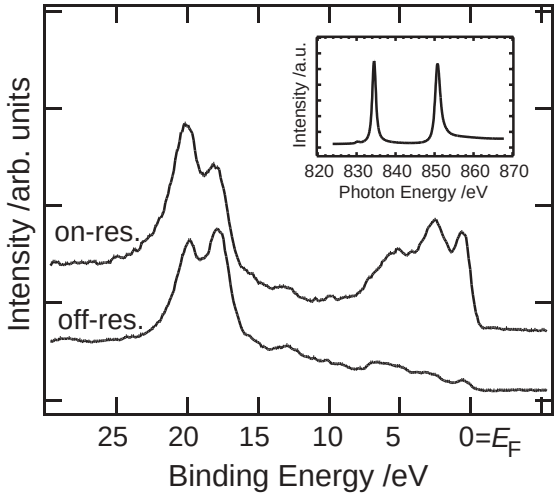

Figure 1. Off- and on-resonant valence-band photoelectron spectra of LaB_2C_2. La 3d-4f photoabsorption spectrum of LaB_2C_2 is also indicated in the inset.

VI-B-2 Cu L-Edge X-Ray Absorption Spectra of $(Me_2\text{-DCNQI})_2Li_{1-x}Cu$

HATSUI, Takaki; TAKATA, Yasutaka[1]; KOSUGI, Nobuhiro; YAMAMOTO, Takashi[2]; TAJIMA, Hiroyuki[2]
([1]RIKEN; [2]Univ. Tokyo)

Cu L-edge X-ray absorption spectra for $(Me_2\text{-DCNQI})_2Li_{1-x}Cu_x$ alloys (Me_2-DCNQI: 2,5-dimethyl-N,N'-dicyanoquinonediimine) were measured at room temperature in order to investigate the local electronic structure around Cu atoms. Total electron yield mode was used except for the alloyed sample with $x < 0.1$, which was obtained by measuring the partial fluorescence yield. Both in the Cu L_3- and L_2-edge regions of $(Me_2\text{-DCNQI})_2Cu$ ($x = 1$) shows a characteristic higher-energy broad band B in addition to a lowest sharp band A associated with the transitions to the Cu 3d hole, while $K_3Cu(CN)_4$ with Cu $3d^{10}$ shows only a higher-energy band E (Figure 1). The broad band B arise from the transitions to the lowest unoccupied molecular orbital (LUMO) of Me_2-DCNQI molecules, where the intensity comes from the Cu 3d components through strong hybridization with Cu. The spectral feature does not change even if the x value (the Cu content) is reduced to less than 0.1. This indicates that these alloys have nearly the same covalent bond between Cu and Me_2-DCNQI as $(Me_2\text{-DCNQI})_2Cu$ ($x = 1$).

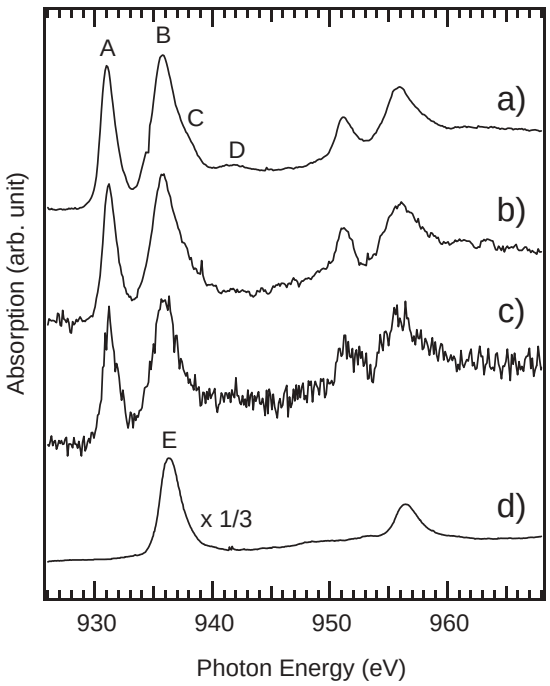

Figure 1. Cu L-edge X-ray absorption spectra of $(Me_2\text{-DCNQI})_2Li_{1-x}Cu_x$ with $x = 1$ (a), $x = 0.15$ (b), and $x < 0.1$ (c). Spectrum of $K_3Cu(CN)_4$ is presented for comparison (d).

VI-B-3 Resonant Inelastic X-Ray Scattering of Ni Dimethylglyoxime

HATSUI, Takaki; KOSUGI, Nobuhiro; RUBENSSON, Jan-Erik[1]; KÄÄMBRE, Tanel[1]; NORDGREN, Joseph[1]
([1]Uppsala Univ.)

In our previous study, we found two metal-to-ligand charge transfer (MLCT) transitions in the Ni L-edge X-ray absorption spectrum of a planar Ni complex, Ni dimethylglyoxime [$Ni(Hdmg)_2$]. The MLCT transition was proved to have close correlation with the π-backbonding. The presence of core hole in the final states of x-ray absorption, however, makes it difficult to obtain quantitative information on the bonding between metal and ligand. On the other hand, the final states of resonant x-ray inelastic scattering (RIXS) correspond to valence-excited states without core hole. In the present study, we have measured RIXS of $Ni(Hdmg)_2$ in order to clarify the bonding nature quantitatively.

Figure 1 shows RIXS spectra (a) and (b) at the higher-energy MLCT excitation. In the E_{in} // k_{out} (E_{in}: electric vector of incident x-ray, k_{out}: wavevector of emitted x-ray) geometry, the band at 860 eV is very weak in accordance with the selection rule, where the direct recombination is symmetry forbidden. The spectrum (c), obtained at the excitation far above the

ionization threshold, is similar to the resonant spectra (a) and (b). Compared with the E_{in} // k_{out} spectrum, peak position of the strongest peak in the $E_{in} \perp k_{out}$ spectrum (a) is shifted toward lower energy side. Based on the consideration of the selection rule and the electronic structure, the shift arises from different one-electron excitations, and the most intense peak in spectra (a) and (b) is revealed to have final states with $(\text{Ni } 3d)^{-1}(\text{ligand } \pi^*)^1$.

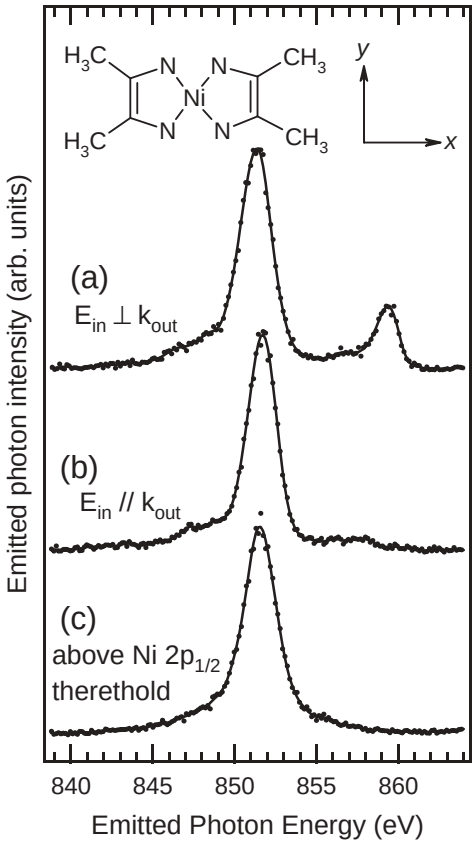

Figure 1. Resonant inelastic X-ray scattering of $Ni(Hdmg)_2$ at the excitation of MLCT band with the $E_{in} \perp k_{out}$ (a) and E_{in} // k_{out} (b) geometries. A non resonant spectrum is shown for comparison (c).

VI-C Observation of Vibrational Coherence (Wavepacket Motion) in Solution-Phase Molecules Using Ultrashort Pulses

With recent remarkable improvements of ultrashort-pulse lasers, we are now able to generate an optical pulse shorter than a few tens of femtoseconds. Owing to its ultrashort duration and broad frequency bandwidth, the ultrashort pulse can excite a molecule 'impulsively' to generate a coherent superposition of vibrational eigen states either in the excited state or in the ground state. This vibrationally coherent state evolves in time, which is called wavepacket motion. The observation and control of the wavepacket motion is one of the most interesting topics in modern spectroscopy. In this project, we study vibrational coherence in the condensed-phase molecules by using ultrashort optical pulses whose duration is ten ~ a few tens of femtoseconds. In this year, we attained the observation of the wavepacket motion in a photo-dissociating molecule in solution, and succeeded in measuring impulsive stimulated Raman scattering form the excited state of a polyatomic molecule for the first time.

VI-C-1 Observation of Coherent Nuclear Motion in the Photoinduced Ring-Opening Reaction of Diphenylcyclopropenone

TAKEUCHI, Satoshi; TAHARA, Tahei[1]
([1]IMS and RIKEN)

When the time-resolution in time-resolved spectroscopy exceeds the period of molecular vibrations, we have a chance to observe the nuclear motions in real time. Thanks to recent progresses in short-pulse lasers, the observation of such a coherent nuclear dynamics becomes possible even during fast chemical reactions. Here, we report on our time-resolved absorption study of the coherent vibrational dynamics in the reaction of diphenylcyclopropenone (DPCP). This molecule has a highly strained three-membered ring structure. It is known that photo-excitation of DPCP causes a dissociation of the carbonyl group, giving rise to diphenylacetylene (DPA) as a product. From our sub-picosecond transient absorption measurements, we concluded that this ring-opening reaction starts form the S_2 state of DPCP, generating the product DPA in the electronically excited (S_2) state. In order to examine the nuclear dynamics during the reaction, we carried out time-resolved absorption measurements with a time resolution as good as 60–70 fs. Figure 1 depicts a temporal behavior of the absorption from the S_2 DPCP, the precursor of the reaction. The precursor absorption decays with a 0.2-ps time constant as the reaction proceeds, which is followed by a residual absorption decay (9 ps) due to the reaction product (S_2 DPA). In addition to this reaction dynamics, we found a weak but significant oscillatory modulation superposed on the decay of the precursor absorption. This modulation arises from the vibrational coherence created by the photoexcitation. The modulation period (110 fs) corresponds to a vibrational frequency of *ca.* 300 cm^{-1}. We concluded that the DPCP exhibits a coherent nuclear motion having the 300-cm^{-1} frequency during the ring-opening reaction.

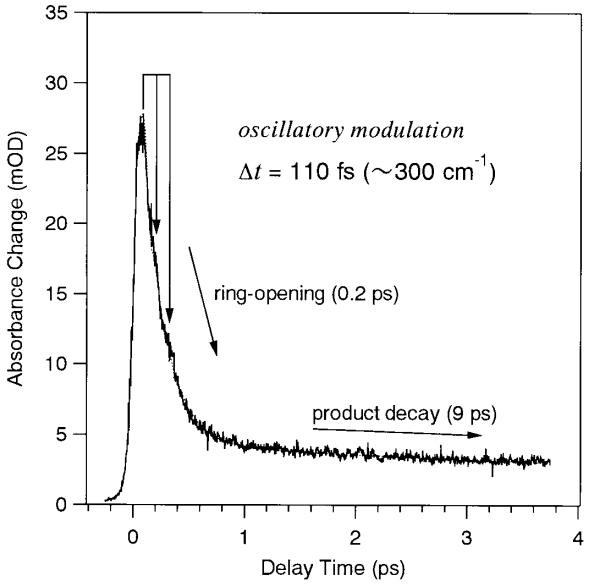

Figure 1. Time-resolved absorption of diphenylcyclopropenone in cyclohexane measured with the 295-nm excitation and 525-nm probe.

VI-C-2 Construction of Transient Resonance Impulsive Stimulated Raman Scattering Spectrometer

FUJIYOSHI, Satoru[1]; TAKEUCHI, Satoshi; TAHARA, Tahei[2]
([1]GUAS; [2]IMS and RIKEN)

Time-resolved spectroscopic study of the low-frequency intra- and inter-molecular vibrations is very important to understand the structure and function of short-lived species such as reaction intermediates. However, observation of low-frequency vibrations by time-resolved frequency-domain Raman spectroscopy is extremely difficult, because a strong Rayleigh scattering often disturbs the measurements. In contrast, it is known that the Rayleigh scattering is readily separated in time-domain Raman methods such as the impulsive stimulated Raman scattering (ISRS) spectroscopy. So far, this ISRS method has been utilized to observe Raman-active low-frequency vibrations of molecular liquids in the ground state. It is highly expected that the ISRS method can also be applied to the observation of

the low-frequency vibrations of transient species. Here, we report our experimental setup constructed for the ISRS spectroscopy of transient species ("transient resonance ISRS").

Figure 1 shows the apparatus used for the transient resonance ISRS measurements. The light source is a Ti:sapphire regenerative amplifier system. The output of this amplifier (800 nm, ~0.1 ps) is divided into two parts. One portion is converted to the third harmonic at 267 nm (~0.5 ps). It is used as a pump pulse, and is focused to the sample jet to generate transient species. Another portion is converted to a visible pulse (600 nm, ~0.04 ps) in an optical parametric amplifier and subsequent frequency doubling. This visible pulse is used for the ISRS process. It is tunable in the 600–800 nm region for best resonance to the absorption of the transient species. The pulse duration of the visible pulse can be as short as 40 fs after the prism compensator. The visible pulse is divided into three, and is focused to the photoexcited portion of the sample jet with a standard BOXCARS geometry. The signal light that is diffracted in the phase matching direction is detected by a photodiode.

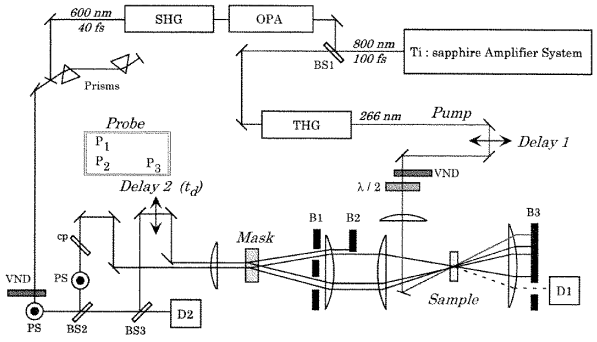

Figure 1. Apparatus of the transient-resonance-ISRS spectrometer.

VI-C-3 Observation of the Low-Frequency Vibration of S_1 *Trans*-Stilbene in Solution Using Transient Resonance Impulsive Stimulated Raman Scattering Method

FUJIYOSHI, Satoru[1]; TAKEUCHI, Satoshi; TAHARA, Tahei[2]
([1]GUAS; [2]IMS and RIKEN)

Recently, we have developed a novel spectrometer for the detection of impulsive stimulated Raman scattering (ISRS) from transient species. By using this transient resonance ISRS method, we measured the low-frequency vibration of excited-state polyatomic molecules in solution, for first time. The ISRS signals obtained from *trans*-stilbene in ethanol are shown in Figure 1. Before photoexcitation (–20 ps), only a weak signal corresponding to the non-resonant electronic response of the solvent was observed (broken line). After photoexcitation (20 ps), in contrast, the intensity of the ISRS signal was strongly enhanced (solid line). The probe wavelength of the ISRS process is in resonance with the $S_n \leftarrow S_1$ transient absorption, so that the enhanced ISRS signal is attributed to S_1 trans-stilbene. The observed ISRS signal of S_1 trans-stilbene consists of a sharp peak, an oscillatory component, and a slowly decaying component. The frequency of the oscillatory component was determined to be 290 cm^{-1} by Fourier analysis, and it is equal to the frequency of an S_1 in-plane bending mode (ν_{24}) that has been observed in time-resolved frequency-domain Raman spectroscopy.[1)] The present measurement successfully demonstrated a high potential of the transient resonance ISRS spectroscopy for the study of low-frequency vibrations of polyatomic molecules in the excited state.

Reference

1) T. L. Gustafson, D. M. Robert and D.A. Chernoff, *J. Chem. Phys.* **81**, 3438 (1994).

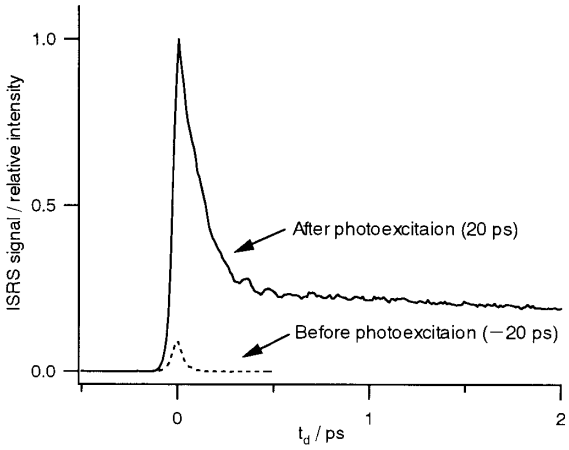

Figure 1. Transient resonance impulsive stimulated Raman scattering signals obtained from *trans*-stlibene in ethanol (pump 266 nm, probe 600 nm).

VI-D Studies of Primary Photochemical/physical Processes Using Femtosecond Electronic Spectroscopy

Ultrafast spectroscopy is playing an essential role in elucidation of photochemical reactions. Thanks to the recent advance in laser technology, we are now able to examine the dynamics of chemical reactions that take place in the femtosecond time region. In this project, we study primary photochemical/physical processes of the condensed-phase molecules using time-resolved fluorescence and absorption spectroscopy whose time-resolution is a few hundreds femtoseconds. Time-resolved fluorescence and absorption spectroscopy are complimentary to each other. The advantage of fluorescence spectroscopy lies in the fact that fluorescence originates from the transition between

the "well-known" ground state and the excited state in question. Thus time-resolved fluorescence spectroscopy can afford unique information not only about the dynamics but also other properties of the excited singlet states such as their energies and oscillator strengths. On the other hand, however, time-resolved absorption spectroscopy is considered to be more versatile because it can detect not only fluorescent excited singlet states but also other "dark" transients. In this year, we investigated the dynamics and mechanism of excited-state proton transfer of hydroxy anthraquinone derivatives, isomerization of trans-azobenzene, and photodissociation of diphenylcyclopropenone. In addition, we obtained a new crucial data about the reaction mechanism of excited-state proton transfer of 7-azaindole dimer.

VI-D-1 Femtosecond Time-Resolved Fluorescence Study of Excited-State Intramolecular Proton Transfer in Hydroxy Derivatives of Anthraquinone

ARZHANTSEV, Sergei; TAHARA, Tahei[1]
([1]IMS and RIKEN)

The proton transfer is one of the most fundamental reactions and plays crucial roles in many processes in chemistry. Anthraquinone is an excellent nucleus for the study of excited state intramolecular proton transfer since the availability of many –OH and $–NH_2$ derivatives and the diversity of positions for substitution. In this study, we chose four α-hydroxy derivatives of anthraquinone: 1-hydroxyanthraquinone (1-HAQ), 1,4-, 1,5-, and 1,8-dihydroxyanthraquinones (DHAQ) to investigate the influence of the second hydroxyl group on photochemistry of molecules.

The steady-state fluorescence spectra of 1-HAQ, 1,5- and 1,8-DHAQs show very large Stokes shift and dual character of emission that is considered as an evidence of the proton transfer reaction in the excited state. In contrast, the fluorescence of 1,4-DHAQ is close to mirror image of absorption. There is no evidence of proton transfer reaction in the excited state.

Femtosecond time-resolved fluorescence intensities of all four molecules in hexane were measured at room temperature for a wide visible wavelength region using up-conversion method. Time-resolved fluorescence spectra were reconstructed after deconvolution taking account of the finite instrumental response. The reconstructed time-resolved fluorescence spectra are presented in Figure 1. We observed the following dynamics for molecules that show dual fluorescence. (1) Both parts of dual fluorescence exist at the time origin. (2) The intensity of short wavelength fluorescence is compatible with intensity of long wavelength fluorescence at the time origin in contrast to the steady-state spectrum. (3) All three molecules show the decrease of short wavelength fluorescence and simultaneous rise of long wavelength fluorescence in the time scale up to 10 ps. (4) In addition, 1-HAQ and 1,5-DHAQ molecules exhibit very fast decay of short wavelength fluorescence intensity in the time scale of 50 fs.

In the case of molecule that shows mirror image type fluorescence (1,4-DHAQ), we found the following dynamics. (1) The spectral changes in the time scale up to 2 ps are similar to spectral changes observed for molecules that exhibit excited state proton transfer. (2) In the time scale from 2 ps up to 50 ps the fluorescence shows the increasing intensity of short wavelength part of the spectrum.

We concluded that proton transfer in α-hydroxy derivatives of anthraquinone is barrierless type of reaction and it occurs in a time scale of several tens of femtoseconds, reflecting delocalization of the excited-state wavefunctions. We assigned the fluorescence dynamics in a few picosecond time scale to an additional proton translocation reflecting the intramolecular vibrational relaxation. It is shown that the excited-state dynamics is affected by position of the second hydroxyl group.

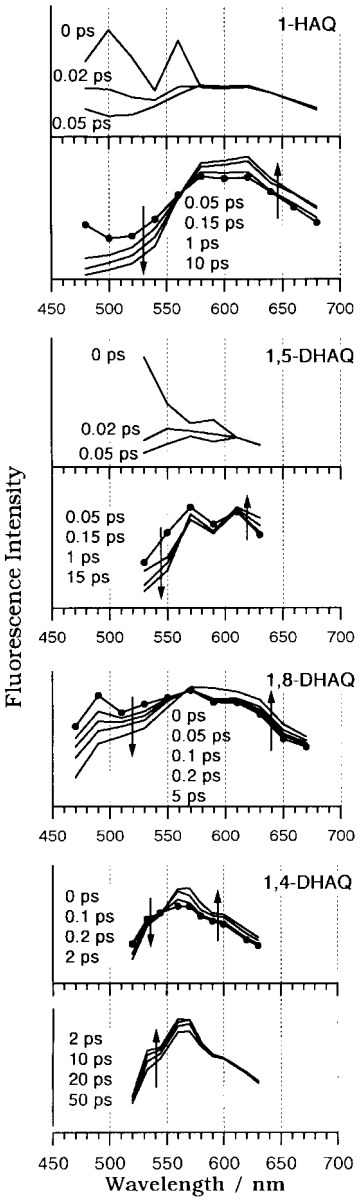

Figure 1. The reconstructed time-resolved fluorescence spectra of hydroxy derivatives of anthraquinone.

VI-D-2 Steady-State and Femtosecond Time-Resolved Fluorescence Study of *Trans*-Azobenzene with $S_2(\pi\pi^*) \leftarrow S_0$ Photoexcitation

FUJINO, Tatsuya; ARZHANTSEV, Sergei; TAHARA, Tahei[1]
([1]IMS and RIKEN)

[*J. Phys. Chem. A* **105**, 8123 (2001)]

Femtosecond time-resolved fluorescence spectroscopy was performed to study the photochemistry of *trans*-azobenzene. Azobenzene in hexane was initially photoexcited to the $S_2(\pi\pi^*)$ state by 280-nm light (560 pJ, 230 fs, 82 MHz) and the time-resolved fluorescence was measured in the wavelength region from 340 to 680 nm by the up-conversion method. The observed fluorescence exhibited double exponential decay and the lifetimes were determined as ~110 and ~500 fs. The spectral analysis of the two fluorescence components showed that their intensity maxima are located at ~400 and ~650 nm. Since they showed good mirror images of the $S_2 \leftarrow S_0$, and the $S_1 \leftarrow S_0$ absorption bands, we assigned them to the fluorescence from the S_2 and S_1 states, respectively, which have planar structure around the central NN bond. The quantum yield of the $S_2 \rightarrow$ 'planar' S_1 electronic relaxation was evaluated by comparing the S_2 and S_1 fluorescence intensities, and it was found to be almost unity. It implies that almost all molecules photoexcited to the $S_2(\pi\pi^*)$ state are relaxed to the 'planar' $S_1(n\pi^*)$ state. The present time-resolved fluorescence study clarified that the isomerization pathway starting directly from the $S_2(\pi\pi^*)$ state does not exist. It was also indicated that the isomerization mechanism of azobenzene is the inversion isomerization occurring in the S_1 state, regardless of difference in photoexcitation conditions.

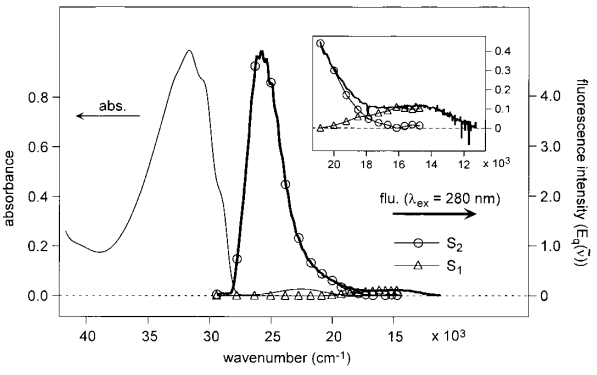

Figure 1. The absorption spectrum (left) and the steady-state fluorescence spectrum obtained with the 280-nm excitation (right). The fluorescence intensity is represented as the photon number intensity in the frequency space. In the fluorescence spectrum, open circles and open triangles represent the S_2 and S_1 fluorescence components, respectively. The wavenumber region from 22000 to 12000 cm^{-1} is expanded in the inset.

VI-D-3 A New Insight into the Relaxation Mechanisms of *trans*-Azobenzene Following the $S_2(\pi\pi^*) \leftarrow S_0$ Photoexcitation: Rotational Deactivation Process from the Vibrationally Excited $S_1(n\pi^*)$ State

FUJINO, Tatsuya; ARZHANTSEV, Sergei; TAHARA, Tahei[1]
([1]IMS and RIKEN)

It is known that the quantum yield of *trans* → *cis* photoisomerization of azobenzene depends on the excitation wavelength: the S_2 excitation gives almost the half value (~0.1) of the S_1 excitation (~0.2). The photoisomerization mechanism of azobenzene has been discussed on the basis of the isomerization quantum yield, and it has been considered that the photoisomerization after the S_2 excitation proceeds differently (rotation) from that after the S_1 excitation (inversion). However, our recent spectroscopic studies clarified that S_2 azobenzene is exclusively relaxed to the 'planar' S_1 state, and hence rotational isomerization pathway from the S_2 state was ruled out. Since it is now clear that the isomerization of azobenzene occurs in the S_1 state regardless of the difference in initial photoexcitation, we need to reconsider the implication of the difference in the isomerization quantum yield between S_2 and S_1 excitation.

After the rapid decay of the S_2 state (~0.11 ps), a considerable amount of photoexcitation energy is localized in the S_1 state in the form of the vibrational excess energy, because vibrational cooling process occurs in a much longer time scale (several tens picosecond). Therefore, a significant difference between S_2 and S_1 excitation is the vibrational excess energy in the S_1 state that appears after photoexcitation. The S_1 state produced after S_2 excitation is highly vibrationally excited (hot) compared to the S_1 state generated by direct S_1 excitation. Thus, the low isomerization quantum yield of S_2 excitation is attributable to the low isomerization efficiency of the vibrationally excited S_1 state. It indicates that another relaxation channel exists especially in the vibrationally excited S_1 state.

It was reported that the isomerization quantum yields obtained with S_2 and S_1 excitation become the same (~0.2) when the rotational motion of azobenzene is prohibited by chemical modification.[1)] This result suggests that the relaxation channel in the vibrationally excited S_1 state is blocked by the chemical modification. In other words, the relaxation channel, which we propose for the vibrationally excited S_1 state, is related to the rotational coordinate, although this channel does not produce the *cis* isomer but generates only *trans* S_0 azobenzene.

Reference

1) H. Rau and E. Lüddecke, *J. Am. Chem. Soc.* **104**, 1616 (1982).

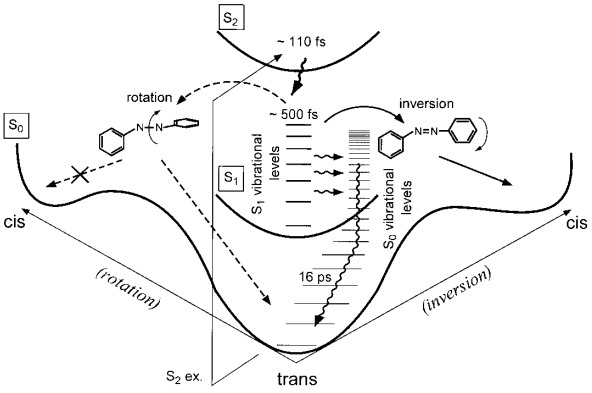

Figure 1. Schematic diagram of the relaxation and isomerization pathway of *trans*-azobenzene after the $S_2(\pi\pi^*) \leftarrow S_0$ photoexcitation.

VI-D-4 Dynamics of Photoinduced Ring-Opening Reaction of Diphenylcyclopropenone Studied by Sub-Picosecond Transient Absorption Spectroscopy

TAKEUCHI, Satoshi; TAHARA, Tahei[1]
([1]IMS and RIKEN)

Since the first synthesis of cyclopropenone derivatives, the aromaticity, stability, and reactivity of their three-membered ring structure have been attracting much interest. Diphenylcyclopropenone (DPCP) is one of the molecules having such a highly strained structure. It is known that photoexcitation of DPCP causes a dissociation of the carbonyl group, giving rise to diphenylacetylene (DPA) as a product (Figure 1). This ring-opening reaction has been studied in solution by picosecond absorption spectroscopy, and it was found that the excited state of DPA is formed by the S_2 excitation of DPCP. However, the ring-opening dynamics itself was not clarified so far because of the low time resolution of the reported measurements (several tens of picoseconds). In this project, we carried out transient absorption measurements with a better (sub-picosecond) time-resolution to elucidate the ultrafast reaction dynamics.

Figure 2 shows transient absorption spectra of DPCP in cyclohexane measured with the S_2 excitation at 267 nm. For comparison, we also plot transient absorption spectra obtained by direct photoexcitation of DPA. It is readily found from this comparison that the DPCP spectra become very similar to the DPA spectra in the delay time region later than 30 ps. This spectral similarity assures that the photoexcitation of DPCP leads to the excited state of DPA. The broad peak around 430 nm recognized in the 30–60 ps time range is due to the S_1 state of DPA generated by the reaction, which then relaxes to the T_1 state (λ_{max} = 410 nm) at later delay times. In the early time region, by contrast, the DPCP spectra are significantly different from the DPA spectra. A strong band is observed around 480 nm just after photoexcitation, which is not seen in the DPA spectra. From its instantaneous rise and fast decay (0.2 ps), we assigned the 480-nm band to the initially-populated S_2 state of DPCP, the precursor of the reaction. This precursor band at 480 nm becomes noticeable only with the good time resolution in the present study. After the fast disappearance of the 480-nm band, the DPCP spectra exhibit a broad feature extending over the entire visible region, which also looks different from the DPA spectra. We tentatively assigned this broad feature to the S_2 DPA generated right after the reaction. The spectral difference seen in the 1–10 ps time range might be due to a reaction-induced structural change of the product DPA in the S_2 state. We conclude that the ring-opening reaction starts from the S_2 DPCP with a 0.2-ps time constant, giving rise to the S_2-like DPA.

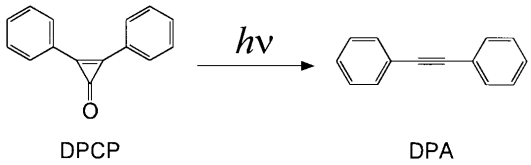

Figure 1. Photoinduced ring-opening reaction of diphenylcyclopropenone.

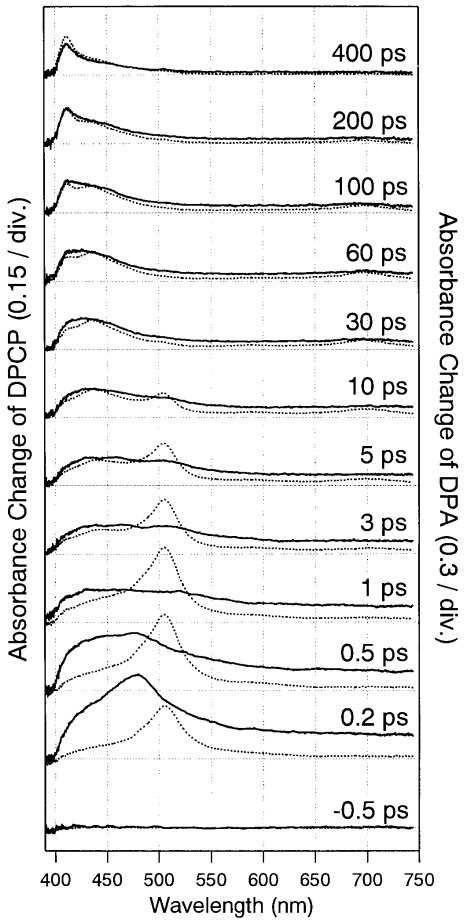

Figure 2. Transient absorption spectra of DPCP (solid) and DPA (dotted) measured in cyclohexane with the 267-nm excitation.

VI-D-5 Excitation-Wavelength Dependence of the Femtosecond Fluorescence Dynamics of 7-Azaindole Dimer: Further Evidence for the Concerted Double Proton Transfer in Solution

TAKEUCHI, Satoshi; TAHARA, Tahei[1]
([1]IMS and RIKEN)

[*Chem. Phys. Lett.* **347**, 108 (2001)]

7-Azaindole dimer is a prototypical system showing the proton transfer reaction in the excited state. It is one of the ideal systems where we can examine the mechanism of the double proton transfer. An important question about the double proton transfer is whether the two protons are translocated in the concerted way or the step-wise way. These two reaction mechanisms have been the subject of intensive debates on the reaction of the 7-azaindole dimer.

Experimentally, it has been confirmed that there exist two components (0.2 ps and 1.1 ps) in the precursor dynamics of the reaction. However, as illustrated in Figure 1, these two components were assigned differently in the discussion that supports each mechanism. In the argument for the concerted mechanism, the 0.2-ps component was assigned to the $S_2 \rightarrow S_1$ electronic relaxation before the reaction and the 1.1-ps component to the actual translocation of the two protons from the S_1 state. On the other hand, in the argument supporting the step-wise mechanism, the 0.2-ps and the 1.1-ps components were assigned to the first and the second proton transfer, respectively. In other words, the two components were attributed to the formation and disappearance of the intermediate in which only one proton is transferred. Therefore, the assignment of the 0.2-ps component is the key to know which mechanism is correct.

In this project, we examined an excitation-wavelength dependence of the ultraviolet fluorescence dynamics. The experiment for the excitation-wavelength dependence is crucial to distinguish the two mechanisms. If the concerted mechanism is relevant, the change of the excitation-wavelength alters the initial population ratio of the S_2 and S_1 states, so that the relative amplitude of the 0.2-ps and 1.1-ps components should change with the excitation-wavelength. In the case of the step-wise mechanism, on the contrary, the relative amplitude of the two components is expected to be constant irrespective of the excitation wavelength, since they correspond to two successive proton-transfer steps. Figure 2 shows fluorescence decays of the dimer excited state(s) (reaction precursor) measured with six excitation wavelengths. It is clear that the precursor dynamics shows a significant excitation-wavelength dependence. In fact, the 0.2-ps component becomes smaller as the excitation wavelength gets longer. Finally, the 0.2-ps component almost vanishes when the dimer is excited at 313 nm, *i.e.*, the red-edge of the dimer absorption. These experimental data are inconsistent with the step-wise mechanism, and deny the existence of the reaction intermediate. We concluded that the proton transfer in solution starts from the S_1 state in the concerted manner with a time constant of 1.1 ps.

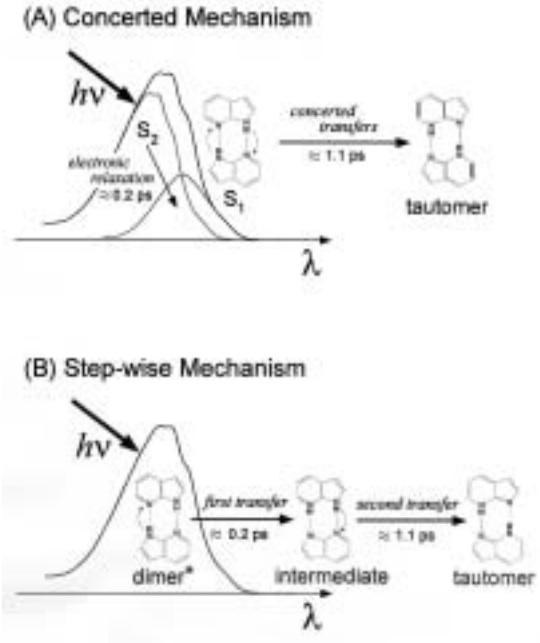

Figure 1. Two reaction mechanisms proposed for the double proton transfer of 7-azaindole dimer.

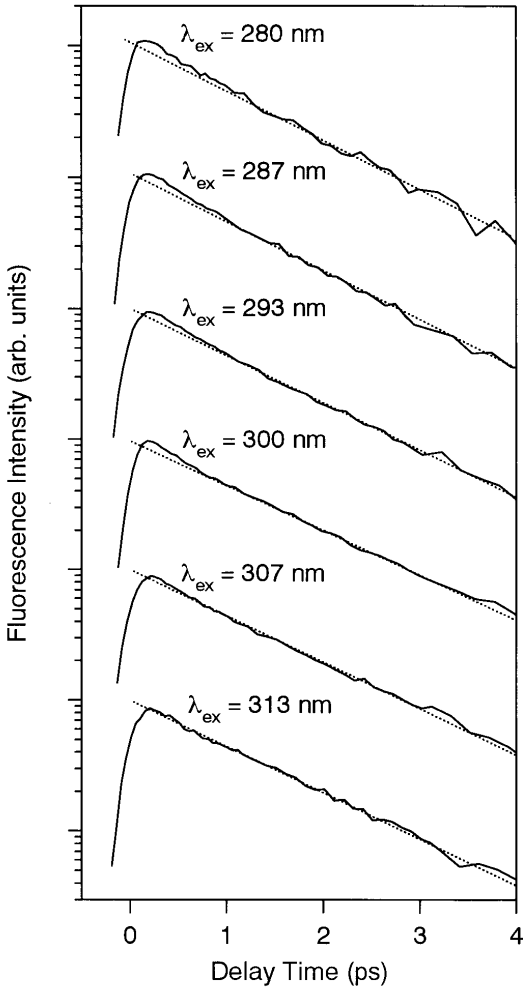

Figure 2. Logarithmic plot of the fluorescence decay of the dimer excited state(s) measured with six excitation wavelengths. The dotted straight line drawn for each data corresponds to a 1.1-ps single-exponential decay.

VI-E Studies of Photochemical Reactions Using Picosecond Time-Resolved Vibrational Spectroscopy

Time-resolved vibrational spectroscopy is a very powerful tool for the study of short-lived transient species. It often affords detailed information about the molecular structure of transients, which is not obtainable with time-resolved electronic spectroscopy. However, for molecules in the condensed phase, we need energy resolution as high as 10 cm^{-1} in order to obtain well-resolved vibrational spectra. This energy resolution is compatible only with time-resolution slower than one picosecond because of the limitation of the uncertainty principle. In this sense, picosecond measurements are the best compromise between energy resolution and time resolution for time-resolved frequency-domain vibrational spectroscopy. In this project, we study photochemical processes and/or short-lived transient species by using picosecond time-resolved Raman spectroscopy. In this year, we studied the solvated electron in water and found a novel resonance Raman enhancement due to the water molecules solvating electrons. For instrumentation, we constructed a new apparatus to perform time-resolved Raman measurements in the near-infrared region. We also demonstrated a new method for temporal fluorescence rejection in Raman spectroscopy and achieved the highest rejection efficiency at the moment.

VI-E-1 Novel Resonance Raman Enhancement of Local Structure around Solvated Electrons in Water

MIZUNO, Misao; TAHARA, Tahei[1]
([1]IMS and RIKEN)

[*J. Phys. Chem. A* **105**, 8823 (2001)]

The solvated electron is the most important basic anionic species in solutions. The absorption maximum of the solvated electron in water is located around 720 nm. This absorption is assigned to the s → p electronic transition of the solvated electron. We measured picosecond time-resolved Raman spectra under the resonance condition with this electronic transition for the first time.

In the experiment, the output of picosecond Ti:sapphire regenerative amplifier was used as the light source for time-resolved Raman measurements. The third harmonic (267 nm) was used to generate solvated electrons. The fundamental pulse (800 nm) was utilized to probe Raman scattering under the condition resonant with the s → p transition of the solvated electron. Figure 1 shows picosecond time-resolved resonance Raman spectra of an indole aqueous solution. Indole is used as the electron seed molecule. A strong transient Raman band appears around 1610 cm^{-1} in accordance with the generation of the solvated electron, while only the weak OH-bend Raman band of bulk water can be observed before the pump pulse irradiation. This transient Raman band is attributable to the vibration of the solvating water molecules that strongly interact with the solvated electron in the first solvation shell. The mechanism of this resonance Raman enhancement was also discussed on the basis of the vibronic theory.

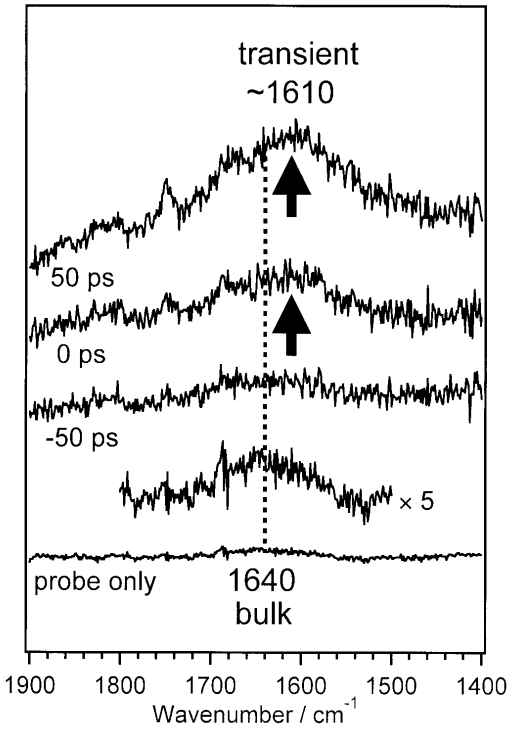

Figure 1. Picosecond time-resolved resonance Raman spectra of water in the presence of indole (1.7×10^{-3} mol dm^{-3}; pump laser 267 nm; probe laser 800 nm). The luminescence background has been subtracted from each spectrum.

VI-E-2 Construction of A Near-Infrared Time-Resolved Raman Spectrometer

MIZUNO, Misao; TAHARA, Tahei[1]
([1]IMS and RIKEN)

Picosecond time-resolved resonance Raman spectroscopy is a very important tool to study the molecular structure of short-lived transient species appearing in photochemical reactions. In order to take advantage of resonance intensity enhancement, the wavelength of the probe light is required to be resonant with the absorption of the transient species. As for the time-resolved Raman measurements in the visible

region, the instrumentation has been already established for both the light source and the detector, and a large number of experiments have been performed. Some important transient species, however, show absorption in the near-infrared region, and near-infrared Raman measurements are needed to study these transients. Therefore, we constructed a new apparatus for near-infrared picosecond time-resolved resonance Raman spectroscopy. The second or third harmonics of the regeneratively amplified output of a picosecond Ti:sapphire laser are used to photoexcite the sample, and the fundamental pulse is used for the probe. Raman scattering is detected by a liquid nitrogen cooled InGaAs multi-channel detector that has sensitivity for the near-infrared light. Figure 1 shows a Raman spectrum of a water-acetonitrile mixture probed by 800 nm, which was measured using the constructed apparatus. We are now able to perform picosecond time-resolved Raman measurement for transient species that shows transient absorption in the near-infrared region.

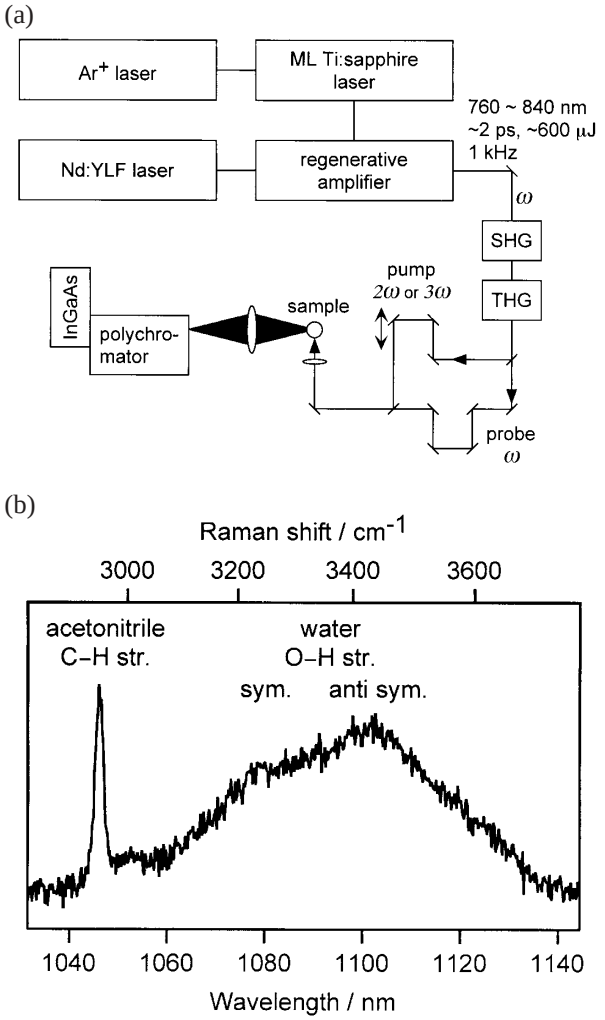

Figure 1. (a) Apparatus for the near-infrared time-resolved Raman spectroscopy. (b) Raman spectrum of a water-acetonitrile (4:1) mixture measured by an InGaAs detector. (probe wavelength 800 nm; laser energy 10 μJ; repetition rate 1 kHz)

VI-E-3 Temporal Fluorescence Rejection in Raman Spectroscopy by the Application of Femtosecond Upconversion Technique

MANDAL, Debabrata; ARZHANTSEV, Sergei; TAHARA, Tahei[1]
([1]IMS and RIKEN)

Temporal fluorescence rejection is a well known and effective method for detecting weak Raman scattering from fluorescent samples. In this method, the temporal response of an ultrafast detection system acts as a "time-gate" to selectively detect the Raman signal, rejecting the longer-lived fluorescence. The efficiency of rejection is proportional to the ratio of fluorescence lifetime and the gating-time. Several techniques have been developed for this purpose, ranging from the use of ultrafast streak camera to applying nonlinear optical effects. But so far, the highest time resolution achieved has been a few picoseconds, using optical Kerr gating technique. We have developed a new method of temporal fluorescence rejection based on femtosecond upconversion. Second harmonic pulses (460 nm) from a Ti:Sapphire oscillator (Tsunami, Spectra Physics) are used to optically excite a solution of acetonitrile containing coumarin 153, a fluorophore with an intense fluorescence having a lifetime of several nanoseconds. The emission from the solution is monitored temporally by the upconversion method using the laser fundamental at 920 nm as the gate pulse. The temporal response of the apparatus is 170 fs, which was given by the fwhm of the cross correlation signal of the gate pulse and the Raman scattering from the neat solvent. Using such a short response time automatically enhances the rejection efficiency by over 1 order of magnitude compared with the previous works.

Excitation at 460 nm causes the Raman lines of acetonitrile to fall within the frequency range of coumarin 153 fluorescence, where they are undetectable in steady-state measurements. However, in the upconversion traces, the Raman response is found to strongly dominate the initial part of the signal at certain emission frequencies (Figure 1). The time resolved emission spectra (TRES) reconstructed from the decays at different emission frequencies clearly exhibit two prominent peaks at ~2250 cm^{-1} and ~2900 cm^{-1} which appear at early delay times (Figure 2a). At slightly later times the peaks vanish, leaving only the fluorescence background (Figure 2b). Comparing the TRES with the Raman spectrum of pure acetonitrile (Figure 2c) recorded with cw excitation, the peaks are assigned to the C–N and C–H stretch Raman bands of acetonitrile respectively. It is noted, however, that both the peaks in the TRES are broadened by almost 200 cm^{-1}. This band broadening results from the inevitable loss of frequency resolution inherent in femtosecond measurements. Nevertheless, our results show that femtosecond upconversion is an efficient solution to the problem of temporal fluorescence rejection in Raman spectroscopy. Additionally, by applying the shortest time-gate for this problem so far, we have achieved an upper limit in the rejection efficiency.

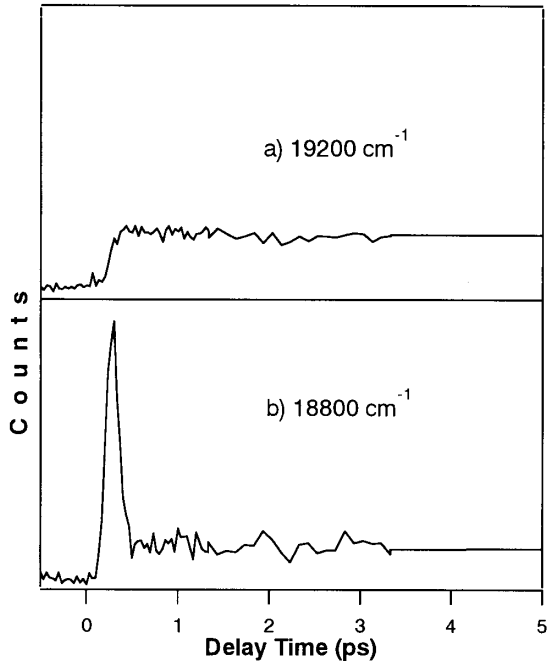

Figure 1. Time-resolved emission of coumarin 153 in acetonitrile at different emission frequencies.

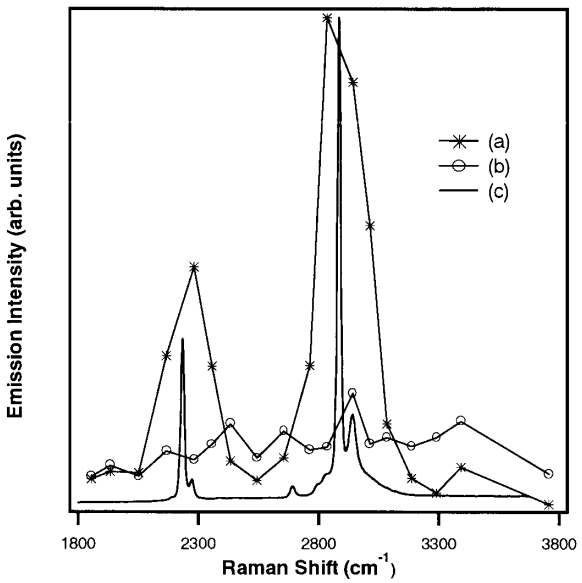

Figure 2. Reconstructed time-resolved emission spectra of coumarin153 in acetonitrile at different time-delays [time res. 160 fs] : a) 50 fs, b) 500 fs, c) Raman spectra of neat acetonitrile (measured with cw excitation).

VI-F Synchrotron Radiation Stimulated Surface Reaction and Nanoscience

Synchrotron radiation stimulated process (etching, CVD) has characteristics of low damage, low contamination, high spatial resolution, and high precision etc. In this project, nanostructures are created by using synchrotron radiation stimulated process, and the reaction mechanisms are investigated by using STM.

VI-F-1 Nanostructure Formation on Si (111) Surface Assisted by Synchrotron Radiation Illumination —Characterization by Scanning Tunneling Microscopy—

NONOGAKI, Youichi; GAO, Yongli[1]; MEKARU, Harutaka[2]; MIYAMAE, Takayuki[3]; URISU, Tsuneo
([1]Univ. Rochester; [2]Himeji Inst. Tech.; [3]Natl. Inst. Mater. Chem. Res.)

[*J. Electron Spectrosc. Relat. Phenom.* **119**, 241 (2001)]

The surface structures after the synchrotron radiation (SR) stimulated removal of native oxide on Si (111) exactly oriented and 4° misoriented surfaces were investigated by scanning tunneling microscopy. The exactly oriented surface showed large regions of atomically flat Si(111)-7×7 structure, and was characterized by the formation of single bilayer steps nicely registered to the underlying crystal structure, clearly different from the disordered step edge obtained by the usual high temperature thermal cleaning. The 4° misoriented sample showed nearly uniformly spaced steps bunched and terraces terminated by 7×7 unit cells in both SR assisted and thermal cleanings, indicating that both cleanings give almost thermal equilibrium surfaces.

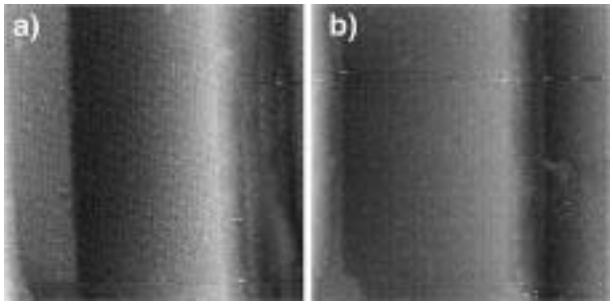

Figure 1. 50 nm × 50 nm STM images of the Si(111) 4° misoriented surfaces after 880 °C 1 min thermal (a), and the 700 °C 2 h SR stimulated cleaning (b), respectively.

VI-F-2 Construction of UHV Variable Temperature STM for *in situ* Observation of SR Stimulated Surface Reaction

NONOGAKI, Youichi; URISU, Tsuneo

We have investigated SR assisted desorption of SiO_2 on Si substrates under the various conditions and have found the significant difference between the thermal and SR-assisted desorption by STM observations. However, these STM images were not taken just after the SiO_2 desoption, since sample setting positions are different between the SR irradiation and STM observation. It is also unclear how the Si surfaces degrade during transferring the samples. To observe the time variation of the surface images more accurately, we have made a new STM system with STM and LEED as shown in Figure 1. By this system, the STM observation and SR irradiation can be conducted at the same sample position.

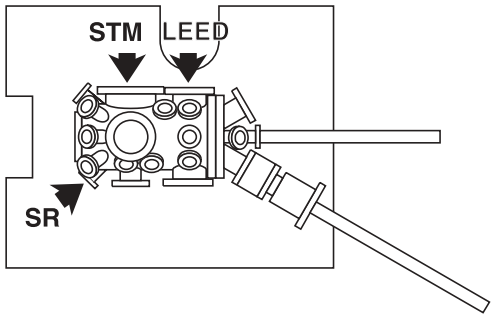

Figure 1. Schematic drawing of new STM system.

VI-F-3 Construction of Low Temperature UHV STM for Observation of Organic- or Bio-Molecules Assembled Silicon Surface

TAKIZAWA, Morio; URISU, Tsuneo

The study on organic- or bio- molecules assembled silicon surfaces is one of the important fields in nano-science. We are now preparing low temperature STM for this purpose. The STM is equiped with VTI unit for temperature control from 2.5 K to R. T. The bio-molecules which are solid, liquid and gas phase materials can be adsorbed by using a small crucible, liquid- and gas- doser, respectively. These evaporators can control a very small amount of exposure to the surfaces. Now, the chamber vacuums are reaching to less than 5.0×10^{-11} Torr (that is detection limit of our ion gauge). Although the condition is not optimized, we have got current-constant images of silicon(111) surface. In the next step, we will observe organic- or bio- molecules assembled on Si(100) surface in UHV.

VI-G Noble Semiconductor Surface Vibration Spectroscopy

As a new high sensitive and high resolution surface vibration spectroscopy technique, we are developing an infrared reflection absorption spectroscopy using buried metal layer substrate (BML-IRRAS). We are now developing a fabrication technique of BML substrate by wafer bonding. We are also investigating several surface chemical reactions on Si surfaces using this BML-IRRAS.

VI-G-1 Initial Stage of Hydrogen Etching of Si Surfaces Investigated by Infrared Reflection Absorption Spectroscopy

NODA, Hideyuki; URISU, Tsuneo; KOBAYASHI, Yoshihiro[1]; OGINO, Toshio[1]
([1]NTT Basic Res. Lab.)

[*Jpn. J. Appl. Phys.* **39**, 6985 (2000)]

The initial stage of etching reactions (breaking the Si–Si back bonds) of Si(100) and Si(111) surfaces exposed to hydrogen at room temperature was investigated by buried metal layer-infrared reflection absorption spectroscopy. The peaks of SiH_2 scissors and SiH_3 deformation modes (< 1000 cm^{-1}) were successfully observed as clear indicators of the initial stage of hydrogen etching reactions. On the Si(100) surface, the hydrogen exposure dependence of these peaks indicated that the etching reaction starts in the relatively low-exposure region of ≥ 300 L (1 L = 1 × 10^{-6} Torr s). We found that the adjacent dihydride is a precursor to breaking the Si back bonds. On the Si(111) surface, it was found that the adatom's two back bonds are easily broken, and that adatom trihydride is generated at a low H-exposure of 70–500 L. Adding to this dominant reaction, the etching of the rest-atom layer was observed at H-exposures higher than 10000 L.

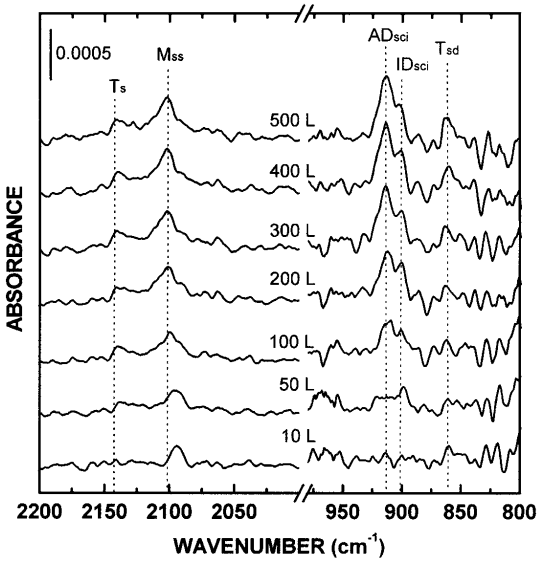

Figure 1. BML-IRRAS spectra of p-polarization for H/Si(100) formed by H-exposure at RT. The resolution is 2 cm^{-1}. H-exposure in units of Langmuir (L) is attached to each spectrum. Peak positions of SiH_n vibration modes are indicated by dotted lines. (M_{ss}: SiH symmetric stretching, T_s: SiH_3 stretching, T_{sd}: SiH_3 symmetric deformation, ID_{sci}: isolated SiH_2 scissors, AD_{sci}: adjacent SiH_2 scissors)

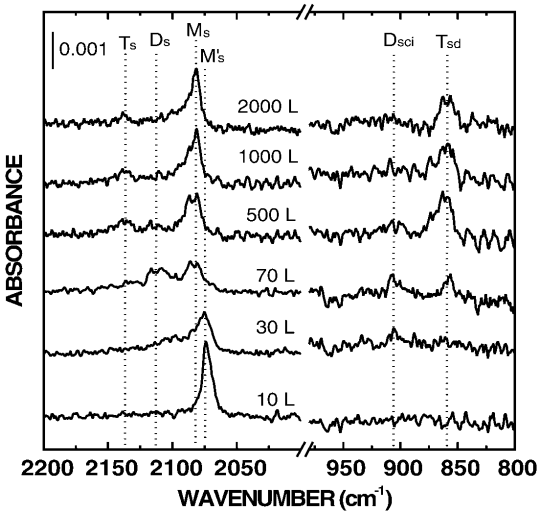

Figure 2. BML-IRRAS spectra of p-polarization for H/Si(111) formed by H-exposure at RT. The resolution is 2 cm^{-1}. H-exposure in units of L is attached to each spectrum. Peak positions of SiH_n vibration modes are indicated by dotted lines. (M_s': SiH stretching of adatom site, M_s: SiH stretching of rest-atom site, D_s: SiH_2 stretching, T_s: SiH_3 stretching, T_{sd}: SiH_3 symmetric deformation, D_{sci}: SiH_2 scissors)

VI-G-2 Nearly Ideally H-Terminated Si(100) Surfaces and IR-Line Width Broadening due to Hydrogen Diffusion into the Subsurface

WANG, Zhihong; NODA, Hideyuki; NONOGAKI, Youichi; URISU, Tsuneo

[*Surf. Sci.* submitted]

Infrared reflection absorption spectroscopy using the buried metal layer substrate (BML-IRRAS) is known to be an unique vibration spectroscopy having a high sensitivity and a high resolution in the wide energy range covering the finger print regions on the semiconductor surfaces. In the present work, dependence of the line width with the coupled monohydride symmetric stretching vibration of the H-terminated Si(100) surface on the adsorption temperature and the hydrogen exposure are investigated by BML-IRRAS method. (Figure 1) The line width significantly changes depending on the adsorption temperature and hydrogen exposure. The reason of the line width broadening is discussed, and it is strongly suggested that the hydrogen diffusion into the subsurface of Si has a significant influence on the line width broadening. The evidence of hydrogen (deuterium) diffusion into the subsurface is investigated for the first time by using IRRAS measurement.

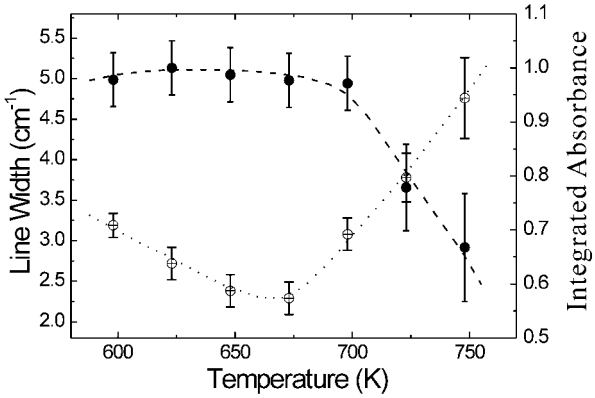

Figure 1. Dependence of line-width (○) and integrated absorbance (●) of the Si–H symmetric stretching peak on the hydrogen atom adsorption temperature.

VI-G-3 Hydrogen Diffusion and Water Reaction on the H-Terminated Si(100) Surface

WANG, Zhihong; NONOGAKI, Youichi; URISU, Tsuneo

[*Jpn. J. Appl. Phys.* submitted (2001)]

Hydrogen terminated Silicon surfaces are interesting not only from the physical studies but also from the application to semiconductor device fabrication. It is known that ideally hydrogen terminated Si(111) surface can be obtained both by wet and dry process and its passivation effects are well investigated. It is also known that the atomically flat hydrogen terminated Si(100) surface is not obtained by wet processes and the chemical reactivity of the hydrogen terminated Si(100) surfaces is also not well understood. The diffusion of hydrogen into silicon bulk is important but not well understood yet due to the difficulties of observation on bulk hydrogen. The reaction with water on H-terminated Si(100) surface is interesting from the viewpoint of understanding the first oxidation step of Si(100) surface. The authors studied these phenomena in detail by measuring the surface vibration spectra of H-terminated Si(100) surfaces using the Infrared reflection absorption spectroscopy using the buried metal layer substrate (BML-IRRAS). It has been observed that the IR line-width changes significantly depending on the hydrogen exposure and adsorption temperature. The line-width broadening was explained by diffusion of hydrogen into Si(100) bulk. The ideally H-terminated Si(100) surfaces were made and the reaction with water was also studied. It has been found that the ideally H-terminated Si(100) surface is easily attacked by water as shown in Figure 1. IR spectrum after 1000L water exposure shows that the original SiH vibration peak decrease (2100 cm^{-1}), SiH_2 peaks generate (~900 cm^{-1}) and the surface is oxidized (~1000 cm^{-1} band).

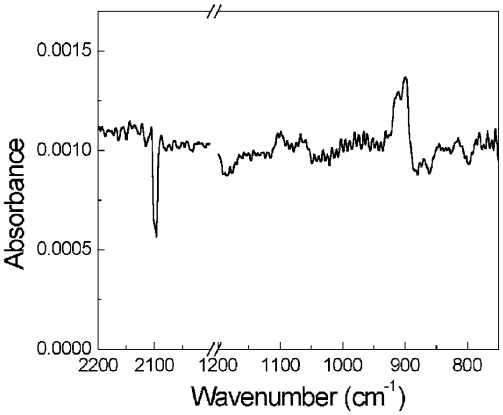

Figure 1. BML-IRRAS spectrum of water reaction with H-terminated Si (100) surface.

VI-H Integration of Bio-Functional Materials on Silicon

Integration of biofunctional materials such as lipids and proteins are expected to find an important applications in biosensors, developments of new medicines, and diagnosis of intractable diseases *etc.* In this project, we are investigating the area selective modification of Si surfaces by depositing the self assembled alkyl monolayers and the characterization by AFM and IRRAS, to integrate biomaterials such as lipids and membrane proteins on Si surfaces with controlled arrangement and orientations.

VI-H-1 Influence of Substrate Roughness on the Formation of Self-Assembled Monolayers (SAM) on Silicon(100)

MORÉ, Sam Dylan; GRAAF, Harald; BAUNE, Michael[1]; WANG, Changshun[1]; NONOGAKI, Youichi; URISU, Tsuneo
([1]Bremen Univ.)

The peak shifts of the CH_2-vibration are an indicator of the amount of gauche-conformational disorder. We have investigated the relationship between surface roughness and morphology and the peak position.

With increasing substrate surface roughness both the symmetric CH_2-peak as well as the asymmetric CH_2-peak shift to higher wave numbers. The magnitude of the shift is about 6 cm^{-1}. The CH_2-peak position correlates with the trans/gauche conformational order in the aliphatic chain.

Scanning electron micrographs showed that the samples which yielded the highest signal intensity exhibited a the highest degree of roughness. This could be confirmed with laser light scattering and qualitatively with profilometer scans.

As trans/gauche oder/disorder and surface density are in close correlation, the insulating properties of

SAM-layers will depend on the microscopic order of the substrate at least for medium length C-chains. Controlling these properties would therefore mandate control of the surface roughness.

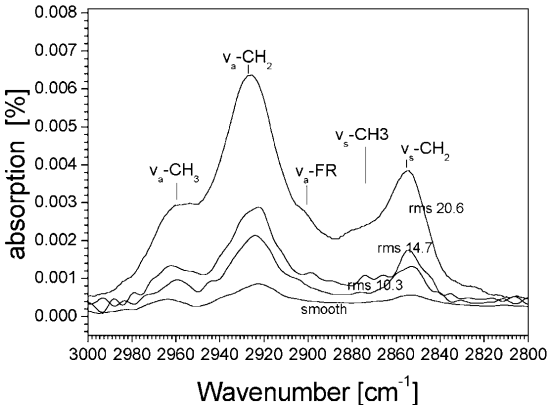

Figure 1. Symmetric (v_s) and asymmetric (v_a) CH_2 and v_a-CH_3 vibrational peaks for the smooth Si(100) and three different roughend Si (100) surfaces (a, b, c), which are covered with a aliphatic self-assembled monolayer. v_a-FR marks a Fermi-resonance and v_a-CH_3 the CH_3 asymmetric peak.

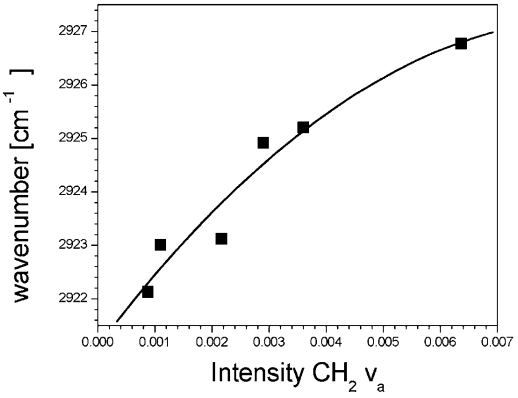

Figure 2. Peak position of the CH_2-asymmetric vibration as a function of peak intensity for an aliphatic SAM (dodecan) on roughened Si(100).

VI-H-2 Characterization of Oligo-Ethylene Glycol Ethers Bound to Self-Assembled Monolayers (SAM) on Silicon with FTIR Spectroscopy and Ellipsometry

MORÉ, Sam Dylan; WANG, Changshun[1]; URISU, Tsuneo

Amphiphilic molecules bound to self assembled monolayers (SAM) can serve as anchor molecules for supported lipid membranes. The resulting anchor entities, bound covalently to the Si-substrate, increase the non-covalently interaction of the lipid with its SAM sublayer, thus enhancing the mechanical stability of the system. Oligo-ethylene glycol molecules, which have been bound to an aliphatic chain are of special interest as the polar chain can further provide hydrophilic pockets to accommodate membrane proteins.

Two different approaches were investigated: Firstly, binding Poly-oxyethylene stearyl ethers to preexisting functionalized self-assembled monolayers on Si(100) via an ester bond and secondly to graft undecenyl acid Brij-esters via the double bond directly to a H terminated Si(100) surface.

Only Poly-oxyethylene stearyl ethers with oxy-ethylene chainlengths of n ($O–CH_2–CH_2$) = 2 and 10. Longer chainlengths (n = 20, 23, 100) could however be attached via the direct grafting method.

Both methods lead to a significant amount of highly ordered Poly-oxyethylene stearyl domains.

VI-H-3 Deposition of Self-Assembled Alkyl Monolayers on Si and SiO_2

WANG, Changshun[1]; MORÉ, Sam Dylan; URISU, Tsuneo
([1]IMS and Henan Univ.)

Preparations of alkyl monolayers on Si and SiO_2 are technologically important for their potential utility. We have deposited octadecyltrichlorosilane (OTS) self-assembled-monolayers (SAM) on silicon substrates with a native oxide (nominally SiO_2) layer. Structural features of the films were characterized using Fourier transform infrared spectroscopy (FTIR) and ellipsometry. The adsorption temperature dependency of FTIR frequencies and intensities of CH_2 stretching vibration bands indicate the existence of a characteristic temperature T_c. The hydrocarbon chains observe an ordered and closely packed state when the monolayers are prepared below T_c, whilst disordered monolayers with low molecular density are formed above T_c. Moreover, dense, well-ordered alkyl SAMs are prepared on the silicon surface by the reactions of neat and dilute 1-alkenes (dodecene, octadecene, *etc.*) with the hydrogen-terminated silicon surface. The hydro-silylation reaction results in the formation of very stable silicon-carbon bonds, which yield dense monolayers as evidenced from infrared spectroscopy and ellipsometry. And the reaction is more efficient at higher temperatures than that at lower temperatures, as shown in Figure 1.

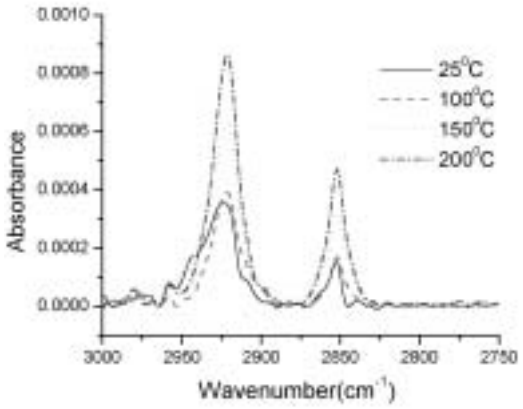

Figure 1. FTIR spectra of SAM obtained from the reaction of pure dodecene with the hydrogen-terminated Si (100) surface at different solution temperatures.

VI-I Photoionization and Photodissociation Dynamics Studied by Electron and Fluorescence Spectroscopy

Molecular photoionization is a major phenomenon in vacuum UV excitation and provides a large amount of information on fundamental electron-core interactions in molecules. Especially, neutral resonance states become of main interest, since they often dominate photoabsorption cross sections and lead to various vibronic states which are inaccessible in direct ionization. We have developed a versatile machine for photoelectron spectroscopy in order to elucidate dynamical aspects of superexcited states such as autoionization, resonance Auger decay, predissociation, vibronic couplings, and internal conversion. Two-dimensional photoelectron spectroscopy, allows us to investigate superexcited states in the valence excitation region of acetylene, nitric oxide, carbonyl sulfide, sulfur dioxide and so on. In this method, the photoelectron yield is measured as a function of both photon energy and electron kinetic energy (binding energy). The spectrum, usually represented as a contour plot, contains rich information on photoionization dynamics.

Photofragmentation into ionic and/or neutral species is also one of the most important phenomena in the vacuum UV excitation. In some cases, the fragments possess sufficient internal energy to de-excite radiatively by emitting UV or visible fluorescence. It is widely accepted that fluorescence spectroscopy is an important tool to determine the fragments and to clarify the mechanisms governing the dissociation processes of diatomic and polyatomic molecules. This year we have carried out fluorescence spectroscopy of OCS in the photon energy region of 15–30 eV.

VI-I-1 Formation and Autoionization of a Dipole-Forbidden Superexcited State of CS_2

HIKOSAKA, Yasumasa[1]; MITSUKE, Koichiro
([1]Inst. Mater. Struct. Sci.)

[*J. Phys. Chem. A* in press]

Two-dimensional photoelectron spectroscopy has been performed in the photon energy region of 14.60–15.35 eV, in order to investigate forbidden superexcited states of CS_2. Figure 1 shows a two-dimensional photoelectron spectrum for the $CS_2^+(\tilde{B}^2\Sigma_u^+)$ band and its vicinities. The electron yield is presented as a function of both photon energy $E_{h\nu}$ and ionization energy I_E by the plots with eight tones from light to dark on a linear scale. The curve in the right panel shows a constant ionic state spectrum, which is obtained by summing electron counts along the I_E axis at each $E_{h\nu}$. Five resonances of the Rydberg states converging to $CS_2^+(\tilde{C}^2\Sigma_g^+)$ are observed at $E_{h\nu}$ = 14.69, 14.88, 14.95, 15.09, and 15.31 eV. The former two states are first assigned in this work. There exists remarkable vibrational excitation of one quantum of the antisymmetric vibrational mode at $E_{h\nu}$ ~ 14.88 eV. A similar excitation can be seen in the two-dimensional spectrum for the $CS_2^+(\tilde{X}^2\Pi_g)$ band. This vibrational excitation is attributable to autoionization from a dipole-forbidden superexcited state which is formed through vibronic interaction with the $5p\sigma_u$ Rydberg state converging to $CS_2^+(\tilde{C}^2\Sigma_g^+)$. The forbidden superexcited state is assigned as the v = 1 vibrational state in the ν_3 mode of the $3d\sigma_g$ Rydberg member converging to $CS_2^+(\tilde{C}^2\Sigma_g^+)$. Preference in the autoionization of the forbidden superexcited state was discussed.

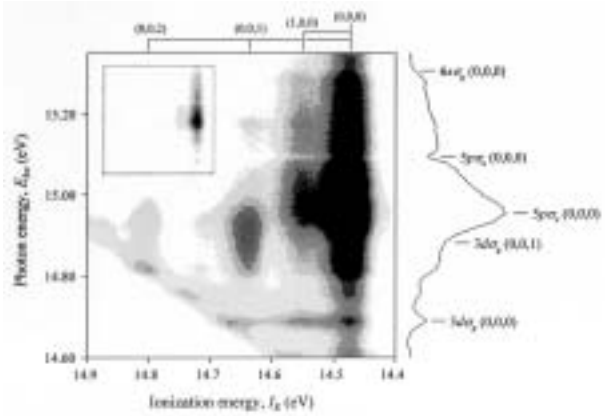

Figure 1. Two-dimensional photoelectron spectrum for the $CS_2^+(\tilde{B}^2\Sigma_u^+)$ band and its vicinities measured in the photon energy range of 14.60–15.35 eV.

VI-I-2 UV and Visible Emission Spectra from Photodissociation of OCS Using Synchrotron Radiation at 15–30 eV

MITSUKE, Koichiro

Photofragmentation of OCS in the excitation photon energy range of 15–30 eV has been studied by dispersed fluorescence spectroscopy using monochromatized undulator radiation supplied from the UVSOR facility. Figure 1 shows dispersed fluorescence spectra of OCS encompassing the wavelength region of 360–530 nm at five photon energies between 19.85 and 29.8 eV. The following emission band systems have been identified: OCS^+ $[A^2\Pi_\Omega(0,0,0) \rightarrow X^2\Pi_\Omega(0,0,\nu_3'')]$, CO^+ $(A^2\Pi_\Omega \rightarrow X^2\Sigma^+)$, CS^+ $(B^2\Sigma^+ \rightarrow A^2\Pi_\Omega)$, and CO $(d^3\Delta \rightarrow a^3\Pi)$. All the transitions except OCS^+ $[A^2\Pi_\Omega \rightarrow X^2\Pi_\Omega]$ are newly obtained from photodissociation of OCS in the vacuum UV region. The fluorescence excitation spectra for the OCS^+ $[A^2\Pi_\Omega(0,0,0) \rightarrow X^2\Pi_\Omega(0,0,\nu_3'')]$ and CS^+ $(B^2\Sigma^+ \rightarrow A^2\Pi_\Omega)$ transitions were measured in the photon energy range of 15.1–15.75 and 21.8–26 eV,

respectively. The emission spectra obtained at 20.85 and 22.9 eV exhibit atomic transitions of S [$nd^3D^o \rightarrow 4p^3P^e$ (n = 6–9)] which result from neutral dissociation of superexcited Rydberg states of OCS into S (nd^3D^o) + CO. Possible excited states of the counterpart CO were discussed on the basis of the difference in the n distribution between the two spectra.

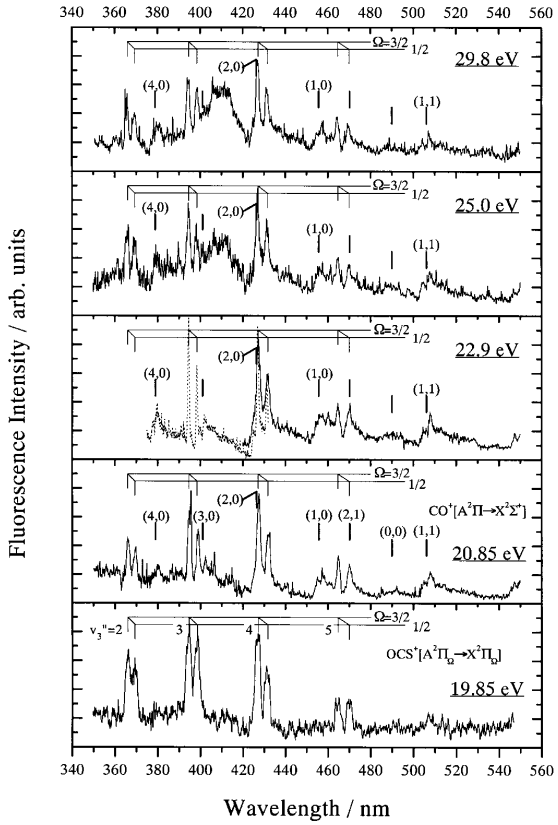

Figure 1. Dispersed fluorescence spectra of OCS encompassing the wavelength region of 360–530 nm at five photon energies between 19.85 and 29.8 eV. The thin vertical lines indicate the vibrational progression in the antisymmetric stretch ν_3 mode of the OCS^+ [$A^2\Pi_\Omega(0,0,0) \rightarrow X^2\Pi_\Omega(0,0,\nu_3'')$] transition. The thick vertical lines indicate the band origins of the CO^+ ($A^2\Pi_\Omega$, $\nu' \rightarrow X^2\Sigma^+$, ν'') emission-band system.

VI-J Development of a Laser-Synchrotron Radiation Combination Technique to Study Photoionization of Polarized Atoms

In conventional photoionization experiments, the most standard method has generally been taken to be measurement of energy and angular distributions of photoelectrons from randomly oriented (unpolarized) atoms or molecules. However, information obtained from these experiments is insufficient, since the initial state constituted of atoms and photons is not selected and the internal properties of final photoions and electrons are not analyzed. In this project, we have performed photoelectron spectroscopy of polarized atoms using linearly-polarized laser light, aiming at complete quantum-mechanical photoionization experiments. Initial excitation with a linearly polarized synchrotron radiation permits ensemble of atoms to be aligned along the electric vector of the light. From an angular distribution of photoelectrons from polarized atoms, we are able to gain insight into the magnitude and phase shift difference of transition dipole matrix elements of all final channels which are allowed by selection rules.

VI-J-1 Development of a Conical Energy Analyzer for Angle-Resolved Photoelectron Spectroscopy

IWASAKI, Kota[1]; MITSUKE, Koichiro
([1]Shimadzu Co.)

[*Surf. Rev. Lett.* submitted]

A new angle-resolving electron energy analyzer composed of a conical electrostatic prism and position sensitive detector has been developed for gas-phase photoelectron spectroscopy. Performance tests have

been made in the energy and angular resolutions, transmission efficiency, and background level of the analyzer. Helium I photoelectron spectroscopy of Ar atoms was employed for the tests (E_{hv} = 21.22 eV). We fabricated a calibration cone electrode, on which a series of apertures of 0.5–2.0 mm in diameter are located as the test objects, and fitted this electrode in the analyzer to check the focussing efficiency by observing photoelectrons that pass through the apertures.

The 5.3 and 5.5 eV electrons produced by photoionization of Ar into $Ar^+(^2P_{3/2,1/2})$ were decelerated or accelerated and were made to pass through the analyzer. The photoelectron spectra were obtained by scanning the potential between the gas cell and inner cone electrode while the transmission energy is kept constant. The two peaks of the $Ar^+(^2P_{3/2,1/2})$ bands manifest symmetric Gaussian profiles, which reveals that the electric field acting upon the photoelectrons from the gas cell was not distorted. We have measured the energy resolution as a function of the transmission energy. The best energy resolution of 60 ± 1 meV (FWHM) has been achieved.

The angular resolution was evaluated from the extent of the image of the entrance apertures on the PSD detector. Figure 1 shows a typical electron image. Three spots correspond to the three entrance apertures of 1.5 and 2 mm in diameter. The angular resolution of 3° (FWHM) was estimated from the spot size for the aperture of 1.5 mm diameter. Taking into account the acceptance angle of 5.4° of the aperture from the sample volume, we can conclude that the conical electrostatic prism has a convergence effect on the incident electrons in the azimuth direction. The diameter of the entrance aperture is the major determining factor of the angular resolution.

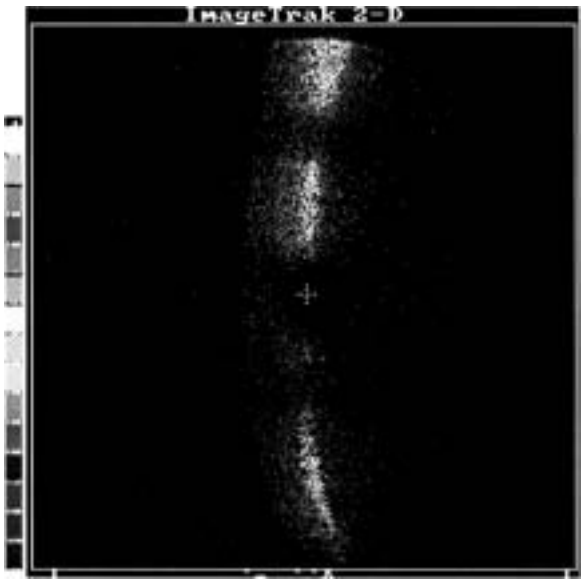

Figure 1. Photoelectron image on PSD. Three spots represent the image of three entrance holes bored on the inner cone electrode. The top spot was cut out by the edge of PSD.

VI-K Vacuum UV Spectroscopy Making Use of a Combination of Synchrotron Radiation and a Mode-Locked or Pulsed UV Laser

An ultraviolet laser system has been developed which synchronizes precisely with the synchrotron radiation (SR) from the storage ring of the UVSOR facility. A mode-locked Ti:sapphire laser is made to oscillate at the frequency of the ring in a multibunch operation mode. The delay timing between SR and laser pulses can be changed from 0 to 11 ns. The following combination studies have been performed: (1) two-photon ionization of helium atoms studied as the prototype of the time-resolved experiment, (2) laser induced fluorescence (LIF) excitation spectroscopy of $N_2^+(X\ ^2\Sigma_g^+)$ ions produced by synchrotron radiation photoionization of N_2 or N_2O, and (3) LIF excitation spectroscopy of $CN(X\ ^2\Sigma^+)$ radicals produced by synchrotron radiation photodissociation of CH_3CN.

VI-K-1 Laser Induced Fluorescence Spectroscopy of CN($X\ ^2\Sigma^+$) Radicals Produced by Vacuum UV Photoexcitation of CH_3CN with Synchrotron Radiation

MITSUKE, Koichiro; MIZUTANI, Masakazu

[*J. Electron Spectrosc. Relat. Phenom.* **119**, 155 (2001)]

Synchrotron radiation-pump and laser-probe spectroscopy is employed to observe CN radicals in the vibronically ground state produced from CH_3CN. The photon energy E_{SR} of synchrotron radiation is changed from 13.6 to 18.6 eV. The laser induced fluorescence signal is measured as a function of E_{SR} with the laser wavelength fixed at the $CN(B\ ^2\Sigma^+, v_B = 0 \leftarrow X\ ^2\Sigma^+, v_X = 0)$ transition. The laser and monitored wavelengths were chosen at 388 and 420.8 nm, respectively. Figure 1 shows a plot of the LIF intensity, the difference between the fluorescence signal counts with and without the laser, as a function of E_{SR}. This plot represents the yield curve for the formation of $CN(X\ ^2\Sigma^+, v_X = 0)$. The onset of 15.4 eV of the fluorescence signal indicates that the detected $CN(X\ ^2\Sigma^+)$ radicals result from dissociative ionization of CH_3CN

$$CH_3CN^+ \rightarrow CN(X\ ^2\Sigma^+) + CH_3^+(X\ ^1A_1'). \quad (1)$$

The partial cross section for the formation of $CN(X\ ^2\Sigma^+)$

is estimated to be 0.1–0.5 Mb and is in a reasonable agreement with that for the CH_3^+ formation.

In contrast to the photoionization efficiency curve of CH_3^+, the LIF signal intensity in Figure 1 rapidly decreases beyond the peak at 15.6 eV and settle down to the background level at > 16 eV. The absence of the LIF signal above 16 eV is ascribed to a large kinetic energy release on the way of the dissociation of CH_3CN^+. The quicker the CN($X\ ^2\Sigma^+$) fragment escapes from the probe region, the lower its time-averaged number density becomes.

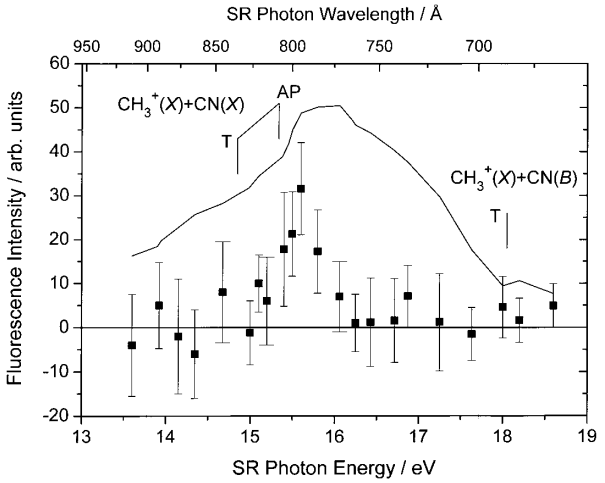

Figure 1. LIF signal intensity (■) of the CN($X\ ^2\Sigma^+$, $v_X = 0$) fragment produced from CH_3CN plotted against the SR photon energy. The solid curve represents the fluorescence excitation spectrum of CH_3CN for the CN(*B*-*X*) emission. In both cases, the ($X\ ^2\Sigma^+$, $v_X = 1$) ← ($B\ ^2\Sigma^+$, $v_B = 0$) transition was monitored.

VI-L Monochromator Newly Developed on the Beam Line BL2B2 in UVSOR

A grazing incidence monochromator has been constructed which supplies photons in the energy region from 20 to 200 eV. This monochromator will bridge the energy gap between the beam lines BL3A2 and BL8B1, thus providing for an accelerating demand for the high-resolution and high-flux photon beam from the research fields of photoexcitation of inner-valence electrons, *L*-shell electrons in the third-row atom, and 4*d* electron of the lanthanides.

VI-L-1 Performance of the 18 m-Spherical Grating Monochromator Newly Developed in the UVSOR Facility

ONO, Masaki; YOSHIDA, Hiroaki[1]; HATTORI, Hideo[2]; MITSUKE, Koichiro
([1]Hiroshima Univ.; [2]Nitto Tech. Inf. Cent. Co.)

[*Nucl. Instrum. Methods Phys. Res., Sect. A* **467-468**, 577 (2001)]

An 18 m-spherical grating monochromator with high resolution and high photon flux has been constructed at the bending magnet beamline BL2B2 of the UVSOR facility in the Institute for Molecular Science. The monochromator covers the energy range of 20–200 eV with three gratings. The resolving power ($E/\Delta E$) has been estimated by ion yield spectra of rare gas atoms (He, Ar and Kr) to be 2000–8000 under the conditions of a photon flux of 1×10^{10} photons s^{-1} and a ring current of 100 mA. A second-order light of 7% is contained at a photon energy of 45.6 eV.

VI-L-2 Anisotropy of Fragment Ions from SF_6 with Valence- and Sulfur *L*-Electron Excitation

ONO, Masaki; MIZUTANI, Masakazu; MITSUKE, Koichiro

Sulfurhexafluoride (SF_6) is one of the most well-known molecules that dissociate to multiple species of fragment ions after photoionization. In this research the asymmetry parameter β of the fragment ion has been measured in the energy region from the outer-valence to sulfur 2*p* electron excitation (23–200 eV).

The apparatus for the measurements of the anisotropy of fragment ions has been constructed at the end station of the beam line BL2B2 of UVSOR. The apparatus consists of two sets of an ion detector and three grids. The two ion detectors were mounted in the parallel and perpendiclar direction to the electric vector of synchrotron radiation. The difference in the sensitivity between the two ion detectors are corrected by measureing the ion yield spectra of hellium and argon atoms.

Figure 1 shows the fragment ion yield from SF_6 and β parameter. The spectrum covers a wide energy range from the outer-valence electron to sulfur 2*p* electron excitation. The three peaks at > 170 eV are assigned to the resonance excitations from $2t_{1u}$ (sulfur 2*p*) to unoccupied valence orbitals ($6a_{1g}$, $2t_{2g}$ and $4e_g$). Several

features around 20–60 eV are found to resemble those in the absorption spectrum. The β parameter decreases with increasing photon energy. This trend can be explained qualitatively by the assumption that SF_5^+ ions has a much more anisotropic distribution than other fragments from SF_6.

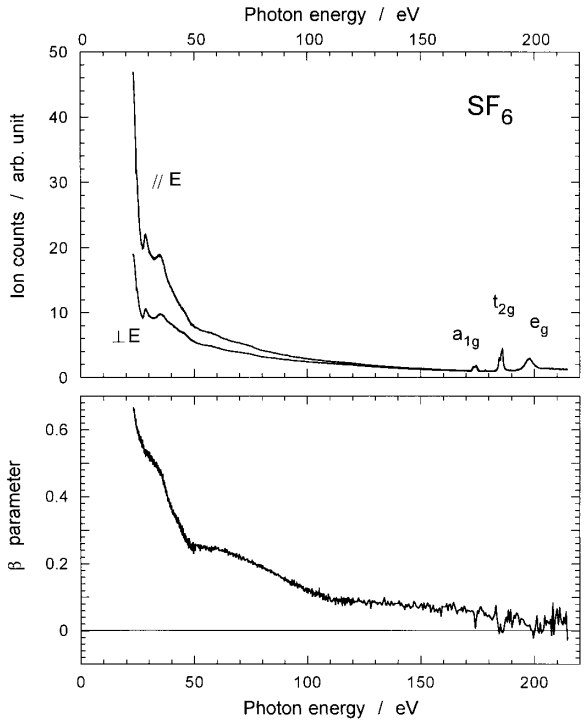

Figure 1. The fragment ion yield spectrum from SF_6 and asymmetry parameter β.

VI-M Thin Film Preparation with Chemical Vapor Deposition Using Vacuum Ultraviolet Radiation

Thin-film deposition at temperatures as low as possible is one of the key technologies for next generation of ultra-large scale integrated circuit (ULSI) fabrication. Photon-assisted chemical vapor deposition is a promising way to prepare particularly dielectric thin films. Silicon dioxide and germanium dioxide films have been prepared from tetraethoxysilane ($Si–(OC_2H_5)_4$) and tetraethoxygermanate ($Ge–(OC_2H_5)_4$) with chemical vapor deposition using vacuum ultraviolet radiation.

VI-M-1 Design and Construction of UVSOR-BL4A2 Beam Line for Nano-Structure Processing

TAKEZOE, Noritaka; YANAGIDA, Hideaki[1]; KUROSAWA, Kou; URISU, Tsuneo; NODA, Hideyuki; MEKARU, Harutaka[2]
([1]IMS and Univ. Miyazaki; [2]Himeji Inst. Tech.)

[*Nucl. Instrum. Methods Phys. Res., Sect. A* **467–468**, 1279 (2001)]

Nano structures must open new windows not only for surface physics and chemistry but also for electronic and photonic devices. Synchrotron radiation stimulated surface chemical reactions have been a most promising way to fabricate nano structures, because they offer a process with the advantages of high-site selectivity by core electron excitation and also free-of damage with atomic scale. Since a new beam line with higher flux is required for the processing, we have been designing and constructing UVSOR-BL4A2 beam line for the nano structure fabrication.

VI-M-2 Characterization of SiO_2 Dielectric Films in Photo-Chemical Vapor Deposition Using Vacuum Ultraviolet Excimer Lamp

TOHIKAWA, Kiyohiko[1]; MIYANO, Junichi[1,2]; MOTOYAMA, Yoshikazu[1,2]; YAGI, Yusuke[1]; YANAGIDA, Hideaki[3]; KUROSAWA, Kou; YOKOTANI, Atsushi[2]; SASAKI, Wataru[2]
([1]Miyazaki Oki Electric Co. Ltd.; [2]Univ. Miyazaki; [3]IMS and Univ. Miyazaki)

[*199th Meeting of Electrochemical Society* **241**]

Photo-chemical vapor deposition using vacuum ultraviolet excimer lamp is a novel technology that deposit SiO_2 film at room temperature without the use of high temperature or plasma. The films contain organic impurities coming from tetraethoxysilane (TEOS) used as the precursor. The addition of O_2 molecules to TEOS is found to decrease C–H impurities. We show atomic concentrations in SiO_2 films deposited from TEOS or from TEOS with O_2 or N_2O gas.

VI-M-3 Electrical Properties of SiO_2 films Prepared by VUV Chemical Vapor Deposition

MOTOYAMA, Yoshikazu[1,2]; MIYANO, Junichi[1,2]; TOSHIKAWA, Kiyohiko[2]; YAGI, Yusuke[2]; KUROSAWA, Kou; YOKOTANI, Atsushi[1]; SASAKI, Wataru[1]
([1]Univ. Miyazaki; [2]Miyazaki Oki Electric Co. Ltd.)

[*199th Meeting of Electrochemical Society* **257**]

We have developed a new scheme for SiO_2-film preparation in which tetraethoxyorthosilicate (TEOS: $Si(OC_2H_5)_4$) is photo-dissociated by vacuum ultraviolet Xe_2 excimer radiation (λ = 172 nm) at room temperature. The SiO_2-films are included impurities of C and H atoms and/or molecules. A adding foreign gases included O atom and molecule to TEOS are effective in removal of C atom and/or molecule in SiO_2-film, which bring about excellent gap-filling property, but it is newly included OH impurity. We had knowledge that the electrical properties of SiO_2-films is correlated the amount of OH impurity by FT-IR spectra, C–V and I–V curves. Increase of OH impurity is degraded electrical properties. An only TEOS have not OH impurity, which may be using as the low-k films of next future device processes.

VI-M-4 SiO_2 Film Deposition on Different Substrate Materials by Photo-CVD Using Vacuum Ultraviolet Radiation

MIYANO, Junichi[1,2]; MOTOYAMA, Yoshikazu[1,2]; TOSHIKAWA, Kiyohiko[2]; YAGI, Yusuke[2]; YANAGIDA, Hideaki[3]; KUROSAWA, Kou; YOKOTANI, Atsushi[1]; SASAKI, Wataru[1]
([1]Univ. Miyazaki; [2]Miyazaki Oki Electric Co. Ltd.; [3]IMS and Univ. Miyazaki)

[*199th Meeting of Electrochemical Society* **258**]

We have prepared SiO_2 thin films from tetraethoxy-orthosilicate (TEOS) at room temperature by photo-chemical vapor deposition using a vacuum ultraviolet (VUV) excimer lamp. We showed the affection by adding foreign gases to the raw precursor and by changing substrate materials for the growth rate and thickness uniformity and the reaction mechanism by step coverage in VUV-CVD. The SiO_2 film deposition behaviors by VUV-CVD depend significantly on the presence of ozone and activated oxygen by VUV photons. Then the dependence of substrate materials for the growth rate and thickness uniformity is most remarkable in case of adding O_2.

VI-M-5 Silica Film Preparation by Chemical Vapor Deposition Using Vacuum Ultraviolet Excimer Lamps

KUROSAWA, Kou; TAKEZOE, Noritaka; YANAGIDA, Hideaki; MIYANO, Junichi[2,3]; MOTOYAMA, Yoshikazu[2,3]; KAWASAKI, Yasuhiro[1]; YOKOTANI, Atsushi[2]
([1]IMS and Univ. Miyazaki; [2]Univ. Miyazaki; [3]Miyazaki Oki Electric)

[*Appl. Surf. Sci.* **168**, 37 (2000)]

We have prepared SiO_2 thin films on silicon wafers from tetraethoxyorthosilicate (TEOS; $Si(OC_2H_5)_4$) by photo-chemical vapor deposition (photo-CVD) with the use of various excimer lamps which emit incoherent light at 308 (XeCl), 222 (KrCl), 172 (Xe_2), 146 (Kr_2) and 126 nm (Ar_2). The film deposition is observed at wavelengths shorter than 172 nm. With 10-mW/cm^2 172-nm radiation, the growth rate is 8 nm/min on the room temperature substrate. The deposition efficiency depends on the wavelength and shows the maximum value for 146-nm radiation. Addition of O_2 to TEOS induces inhibition of C and H impurity inclusion in the films.

VI-M-6 GeO_2 and SiO_2 Thin Film Preparation with CVD Using Ultraviolet Excimer Lamps

KUROSAWA, Kou; MAEZONO, Yoshinari[1]; MIYANO, Junichi[1,2]; MOTOYAMA, Yoshikazu[1,2]; YOKOTANI, Atsushi[1]
([1]Univ. Miyazaki; [2]Miyazaki Oki Electric)

[*J. Phys.* **11**, 739 (2001)]

We have prepared SiO_2 and GeO_2 thin films from tetraethoxyorthosilicate (TEOS; $Si(OC_2H_5)_4$) and tetraethoxyorthogermanate (TEOG: $Ge(OC_2H_5)_4$), respectively, by chemical vapor deposition (CVD) assisted by high-energy photons. The photons are supplied from excimer lamps which emit incoherent light at 308 (XeCl), 222 (KrCl), 172 (Xe_2), 146 (Kr_2) and 126 nm (Ar_2). GeO_2 film deposition is observed for all excimer lamps used here, but SiO_2 films are obtained at wavelengths shorter than 172 nm. This is caused by a fact that the bonding energy between Si and O is much higher than that between Ge and O. The deposition rate is around 8nm/min for SiO_2 and 16nm/min for GeO_2 films. The film deposition rate increases with increasing the light intensity and with decreasing substrate temperature.

VI-M-7 Room Temperature Deposition of GeO_2 Thin Films Using Dielectric Barrier Discharge Driven Excimer Lamps

MAEZONO, Yoshinari[1]; YANAGIDA, Hideaki[2]; NISHI, Kota[1]; MIYANO, Junichi[1,3]; YOKOTANI, Atsushi[1]; KUROSAWA, Kou; HISHINUMA, Nobuteru[4]; MATSUNO, Hiromitsu[4]
([1]Univ. Miyazaki; [2]IMS and Univ. Miyazaki; [3]Miyazaki Oki Electric; [4]USHIO Inc.)

[*J. Phys.* **11**, 811 (2001)]

We discuss the fabrication of GeO_2 and GeO_2/SiO_2 films at room temperature by photo-chemical vapor deposition. Excimer lamps were used for the light source, and tetraethothoxyorthosilicate (TEOS) and tetraethoxyorthogermanate (TEOG), as raw materials. We fabricated GeO_2/SiO_2 composite films from a mixed vapor of TEOS and TEOG. The refractive indices of the obtained films showed intermediate values between those of SiO_2 (n = 1.46) and GeO_2 (n = 1.60). The relationship between Ge concentratipon in the films and the refractive indices was examined. We successfully obtained a GeO_2/SiO_2 composite material of higher refractive index than that of similar composites produced by conventional methods.

VI-N Atoms and Molecules at Water-Zeolite Interfaces: Structure Determination based on AFM Observations

One of the striking capabilities of atomic force microscopy (AFM) is the direct observation of atoms and adsorbed molecules on a surface heretofore impossible, such as nonconductive materials like zeolite, under environments heretofore impossible, including underwater. The unprecedented resolution of AFM imaging enabled us to determine, for the first time, the positions of framework oxygen and extra-framework cation on a (010) surface of heulandite, a zeolite naturally occurring, and the array and the orientation structures of adsorbed molecules on its surface. Based on the *in situ* AFM observations, molecular simulations were performed to supplement the knowledge of aqueous phase adsorption processes.

VI-N-1 High-Resolution Imaging of Organic Monolayers Using Noncontact AFM

UCHIHASHI, Takayuki[1]; ISHIDA, Takao[1]; KOMIYAMA, Masaharu; ASHINO, Makoto[1]; SUGAWARA, Yasuhiro[1,2]; MIZUTANI, Wataru[1]; YOKOYAMA, Kousuke[2]; MORITA, Seizo[2]; TOKUMOTO, Hiroshi[1]; ISHIKAWA, Mitsuru[1]
([1]Joint Res. Cent. Atom Tech.; [2]Osaka Univ.)

[*Appl. Surf. Sci.* **157**, 244 (2000)]

Noncontact atomic force microscopy (AFM) provides useful technique for imaging organic molecules in high resolution. Here we present our recent advances in the noncontact AFM imaging of organic materials. (I) Molecular packing structures, defects and domain boundaries were clearly observed on adenine and thymine films. The noncontact AFM images revealed detailed features of the individual nucleic acid base molecules, thus allowing us to distinguish between adenine and thymine. (II) Both $(\sqrt{3}\times\sqrt{3})R30°$ structures and c(4×2) superlattice structures were resolved on alkanethiolate self-assembled monolayer (SAM) [CH_3-$(CH_2)_8SH$] (nonanethiol) on Au(111). We found that the c(4×2) superlattice structures changed into $(\sqrt{3}\times\sqrt{3})R30°$ structures when the tip-surface distance decreased.

VI-N-2 Study of Catalyst Preparation Processes by Atomic Force Microscopy (AFM): Adsorption of a Pt Complex on a Zeolite Surface

KOMIYAMA, Masaharu; GU, Ning[1]
([1]Southeast Univ.)

[*Stud. Surf. Sci. Catal.* **130**, 3173 (2000)]

Adsorption of a Pt complex commonly used for catalyst preparation onto a (010) surface of a natural zeolite heulandite was examined by *in situ* atomic force microscopy (AFM). The Pt complex appears to adsorb on the heulandite(010) surface at a three-times periodicity along the *c* axis, whereas along the *a* axis no specific periodicity was observed. Possible adsorption sites were also discussed.

VI-N-3 Recent Applications of Atomic Force Microscopy to the Study of Pyridine-Base Molecules Adsorbed on the (010) Surfaces of Heulandite and Stilbite Crystals

KOMIYAMA, Masaharu; SHIMAGUCHI, Takemi[1]
([1]Yamanashi Univ.)

[“*Natural Zeolites for the Third Millennium*,” C. Colella and F. A. Mumpton, Eds., De Frede Editore; Naples p. 315 (2000)]

Liquid-phase adsorption characteristics of pyridine-base molecules, pyridine and β-picoline, on (010) surfaces of two natural zeolites, heulandite and stilbite, were examined by atomic force microscopy (AFM). These adsorption systems formed well-ordered, two-dimensional (quasi-)hexagonal adsorbed layers, with their unit-cell dimensions ranging from 0.48 nm to 0.59 nm depending on the adsorbate-substrate combinations. Although there were near registries of the adsorbed phases with respect to the substrate (010) lattices, the molecular arrays were essentially incommensurate with the substrate atomic arrangements. Orientations of the molecules within the adsorbed layers were determined from the AFM images, which were compared favorably with semiempirical molecular orbital calculations.

VI-N-4 Atomic Force Microscopy Observations of Zeolite(010) Surface Atoms and Adsorbed Molecules

KOMIYAMA, Masaharu

[*Hyomen Kagaku (J. Surf. Sci. Soc. Jpn.)* **21**, 576 (2000)]

Atomic force microscopy (AFM) is capable of directly observating surface atoms and adsorbed molecules on nonconductive materials such as zeolite, under various environments including vacuum, ambient and underwater. We have been successful in observing in situ atomic images of heulandite and stilbite (010) surfaces under aqueous environments, and molecular images of liquid-phase-adsorbed organics on these surfaces. The unprecedented resolution of the AFM imaging enabled us to determine, for the first time, the positions of framework oxygen and extra-framework cation, and the array and orientation structures of adsorbed molecules such as pyridine bases.

VI-O Soft X-Ray, Ultraviolet, Visible and Infrared Spectroscopy of Solids and Devices

Work of soft x-ray(SX), ultraviolet (UV), visible (VIS) and Infrared (IR) spectroscopy of solids have been proceeded. These are mainly performed using synchrotron radiation (beamlines BL7B, BL8B1, BL4B, BL7A and BL1A at UVSOR), owing to the wide wavelength continuity of synchrotron radiation with no structure.

VI-O-1 Reflection Spectra of $Al_{1-x}Ga_xN$

FUKUI, Kazutoshi; MIURA, Hiroshi[1]; OKADA, Akira[2]; GUO, Qixin[2]; TANAKA, Satoru[3]; HIRAYAMA, Hideki[4]; AOYAGI, Yoshinobu[4]
([1]Fukui Univ.; [2]Saga Univ.; [3]Hokkaido Univ.; [4]RIKEN)

Visible, ultraviolet and vacuum ultraviolet reflection spectra of wurtzite $Al_{1-x}Ga_xN$ have been measured from 20 K to 300 K, and Kramers-Kronig analysis using of our results also presented. No drastic change in spectra between GaN and $Al_{0.14}Ga_{0.86}N$. The band gap as the function of temperature has been also presented in whole x range from 20 K to 300 K. They are well described by the Bose-Einstein expression. It suggests that the temperature shift of the band gap is mainly due to the electron-phonon interactions. The parameters of the Bose-Einstein expression are obtained by fitting.

VI-O-2 Characterization of GaN-Based Schottky Barrier Ultraviolet (UV) Detectors in the UV and Vacuum Ultraviolet (VUV) Region Using Synchrotron Radiation

MOTOGAITO, Atsushi[1]; YAMAGUCHI, Motoo[1]; HIRAMATSU, Kazumasa[1]; KOTOH, Masahiro[2]; OHUCHI, Youichiro[2]; TADATOMO, Kazuyuki[2]; HAMAMURA, Yutaka[3]; FUKUI, Kazutoshi
([1]Mie Univ.; [2]Mitsubishi Cable Ind. Ltd.; [3]Nikon Co. Ltd.)

[*Jpn. J. Appl. Phys., Part 2* **40**, L368 (2001)]

Characterization of GaN-based Schottky barrier ultraviolet (UV) detectors with a comb-shaped electrode using synchrotron radiation ($h\nu$ = 2.2–30 eV, λ = 41–563 nm) is described. Below $h\nu$ = 8.0 eV (λ > 155 nm), the detectors are available without any photo-emission of GaN and Au electrode. Under application of reverse bias, the responsivity is increased to 0.05 A/W at ~0.4 V. The photocurrent is controlled by reverse bias. On the other hand, above $h\nu$ = 8.0 eV (λ < 155 nm), the responsivity spectra are dominated by photo-emissions of Au and GaN. These results show that these Schottky type detectors with mesa structures are effective to detect vacuum ultraviolet (VUV)-UV light (155 < λ < 360 nm).

VI-O-3 Near K-Edge Absorption Spectra of the III-V Nitride

FUKUI, Kazutoshi; HIRAI, Ryousuke[1]; YAMAMOTO, Akio[1]; HIRAYAMA, Hideki[2]; AOYAGI, Yoshinobu[2]; YAMAGUCHI, Sigeo[3]; AMANO, Hiroshi[3]; AKASAKI, Isamu[3]; TANAKA, Satoru[4]

([1]Fukui Univ.; [2]RIKEN; [3]Meijo Univ.; [4]Hokkaido Univ.)

[*Phys. Status Solidi B* in press]

The nitrogen and aluminum near K-edge absorption measurements of the wurtzite AlN, GaN and InN, and their ternary compounds (AlGaN, InGaN and InAlN) at various molar fractions have been performed using synchrotron radiation. Using the linear polarization of synchrotron radiation, absorption measurements with different incident light angle also performed. The spectral distribution of the nitrogen K absorption spectra clearly depends on both the incidence light angle and the molar fractions of the samples. That of the aluminum K absorption spectra also show the clear angle dependence, but it does not show the drastic molar dependence. The spectral shape comparisons among the various molar fractions, different incident angles and between two ion sites are discussed. The numerical component analysis of the K absorption spectra is also presented.

VI-P Optical Techniques for Synchrotron Radiation

The performance check of beamline BL7B at UVSOR and the development of a surface profiler for optical elements used in synchrotron radiation beamline have been proceeded

VI-P-1 Performance of IR-VUV Normal Incidence Monochromator Beamline at UVSOR

FUKUI, Kazutoshi; MIURA, Hiroshi[1]; NAKAGAWA, Hideyuki[1]; SHIMOMURA, Iwao[2]; NAKAGAWA, Kazumichi[3]; OKAMURA,

Hidekazu[3]; NANBA, Tadao[3]; HASUMOTO, Masami; KINOSHITA, Toyohiko[4]
([1]Fukui Univ.; [2]JAERI; [3]Kobe Univ.; [4]Univ. Tokyo)

[*Nucl. Instrum. Methods Phys. Res., Sect. A* **467–468**, 601 (2001)]

The beamline BL7B at the UVSOR facility for solid-state spectroscopy has been opening for users after reconstruction. This beamline consists of a 3 m normal incidence monochromator and covers the spectral range from the vacuum ultraviolet to the infrared region. The optical configuration and the performance, such as photon number, purity and resolving power, are reported.

VI-P-2 Development of A Surface Profiler for Optical Elements

KINOSHITA, Toyohiko[1]; FUKUI, Kazutoshi; ASAKA, Shuji; YOSHIDA, Hisashi; WATANABE, Michio; HORIGOME, Toshio[2]; MA, Peijun[3]; OHTSUKA, Ken[3]; IWANAGA, Masanao[3]; OHSHIMA, Eiichi[4]
([1]Univ. Tokyo; [2]JAIST; [3]Canotec Co.,Inc.; [4]Canon Inc.)

[*Nucl. Instrum. Methods Phys. Res., Sect. A* **467–468**, 329 (2001)]

A surface profiler for optical elements used in synchrotron radiation beamlines has been developed. By measuring the precise positions of an incident and reflected laser beam, the surface profile of mirrors and gratings can be obtained. The profile of large mirrors up to 700 mm long and that of any other shape device such as plane and non-spherical mirrors can be also measured. The design concept and preliminary examples of profile measurements are reported.

VI-Q Dynamics and Relaxation of Atoms and Molecules Following Core-Level Excitation

Monochromatized X-ray from synchrotron radiation excites a core electron of an atom or molecule, and the core hole thereby created is usually filled by an outer-orbital electron through an Auger process. In molecules, the core electrons are localized near the atom of origin, in contrast to valence electrons, which are often delocalized over the entire molecule. Although core electrons do not participate in chemical bonding, the energy of an atomic core-level in the molecule depends on the chemical environment of the atom. Site-specific excitation and fragmentation are thus of considerable interest. To elucidate the dynamics and relaxation of atoms and molecules following core-level excitation, we have used photoelectron spectroscopy and the energy-selected-photoemission photoion coincidence method.

VI-Q-1 Site-Specific Fragmentation Following C:1s Core-Level Photoionization of 1,1,1-Trifluoroethane Condensed on a Au Surface and of a 2,2,2-Trifluoroethanol Monolayer Chemisorbed on a Si(100) Surface

NAGAOKA, Shin-ichi; TANAKA, Shin-ichiro[1]; MASE, Kazuhiko[2]
([1]Nagoya Univ.; [2]KEK-PF)

[*J. Phys. Chem.* **105**, 1554 (2001)]

We used photoelectron spectroscopy, the energy-selected-photoelectron photoion coincidence (ESPEPICO) method, the Auger-electron photoion coincidence (AEPICO) method and the ab initio method to study site-specific phenomena in the C:1s photoionization of 1,1,1-trifluoroethane (CF_3CH_3, TFEt) condensed on a Au surface. Site-specific excitation and occurrence of different chemical shifts at two carbon sites were evident in the total electron-yield spectrum and the photoelectron spectrum, and site-specific fragmentation was evident in the ESPEPICO spectrum. The fragmentation processes inferred from the ESPEPICO and AEPICO results were very different from those occurring in the vapor phase. We also studied the effect of the surface on the site-specific phenomena observed in a 2,2,2-trifluoroethanol (TFEtOH) monolayer chemisorbed on a Si(100) surface ($CF_3CH_2OSi\{substrate\}$). The molecular structure of TFEtOH is the same as that of TFEt except that it has a hydroxyl group substituted for one of the hydrogen atoms. Although site-specific phenomena were also observed in TFEtOH, the fragmentation process was very different from that of TFEt because of the chemisorption structure of TFEtOH on Si(100).

VI-Q-2 Si:2p Site-Specific Excitation and Fragmentation of Bridged Trihalosilyltrimethylsilyl Molecules: Role of the Bridge and Final-State Effect

NAGAOKA, Shin-ichi; FUJIBUCHI, Tonan[1]; OHSHITA, Joji[2]; NAGASHIMA, Umpei[3]; KOYANO, Inosuke[4]
([1]Ehime Univ.; [2]Hiroshima Univ.; [3]AIST; [4]Himeji Inst. Tech.)

To elucidate site-specific phenomena, we experimentally and computationally studied the spectroscopy and dynamics caused by Si:2p core-level photoexcitation of bridged trihalosilyl-trimethylsilyl molecules. We used the photoionization efficiency curve and the photoelectron photoion coincidence method to study the site-specific phenomena in the Si:2p photoexcitation of $F_3SiCH_2CH_2CH_2Si(CH_3)_3$, $F_3SiCH{=}CHSi(CH_3)_3$ and $Cl_3SiC{\equiv}CSi(CH_3)_3$ in the vapor phase. The site-specific excitation was revealed in the photoionization efficiency curves of all the molecules. The site-specific fragmentation is likely to be more evident when the distance between the two Si sites is large. For the site-specific fragmentation to occur, there should not be a triple bond between the atomic site of interest and any other near atomic-site around which bond dissociation is undesirable. Not only initial-state effect but also final-state effect is likely to contribute to the occurrence of the different chemical shifts between the two Si sites of the bridged trihalosilyl-trimethylsilyl molecules.

VI-Q-3 Site-Specific Fragmentation Caused by Core-Level Photoionization: Effect of Chemisorption

NAGAOKA, Shin-ichi; MASE, Kazuhiko[1]; NAKAMURA, Arinobu[2]; NAGAO, Masashi[3]; YOSHINOBU, Jun[3]; TANAKA, Shin-ichiro[4]
([1]KEK-PF; [2]Ehime Univ.; [3]ISSP; [4]Nagoya Univ.)

We used the energy-selected-photoelectron photoion coincidence (ESPEPICO) method to clarify site-specific fragmentation caused by C:1s photoionization of 1,1,1-trifluoro-2-propanol-d_1 ($CF_3CD(OH)CH_3$, TFIP-d_1) on a Si(100) surface. The formation of the monolayer was verified by the layer-resolved shifts in the photoelectron and Auger spectra. By using high-resolution electron energy loss spectroscopy, it was shown that TFIP-d_1 is dissociatively chemisorbed like $(CF_3)(CH_3)CDO$-Si(100). Occurrence of different chemical shifts at the three carbon sites was observed by photoelectron spectroscopy. Site-specific fragmentation was clearly revealed in the ESPEPICO spectra of the monolayer at room temperature. From the results of the site-specific fragmentation, it is considered that TFIP-d_1 in the monolayer at room temperature has an O–Si bond oriented in the trans position with respect to the C–CF_3 bond. The fragmentation processes were discussed on the basis of the results of the ESPEPICO method and

the Auger-electron photoion coincidence method.

VI-Q-4 Development of Electron-Ion Coincidence Spectroscopy for Study of Vapor-Phase Dynamics

MASE, Kazuhiko[1]; NAGAOKA, Shin-ichi
([1]KEK-PF)

An electron-ion coincidence spectrometer for vapor-phase dynamics study has been built. The equipment consists of an electron gun, a cylindrical mirror analyzer (CMA) and a reflectron-type time-of-flight ion mass analyzer. Sample gas is excited with the electron beam and the CMA analyzes energy of emitted or scattered electrons. Mass spectra of produced ions are measured with a multichannel scalar taking the energy-analyzed electron signal as the starting trigger.

VI-Q-5 Electron-Ion Coincidence Spectroscopy as a New Tool for Surface Analysis—an Application to the Ice Surface

TANAKA, Shin-ichiro[1]; MASE, Kazuhiko[2]; NAGASONO, Mitsuru; NAGAOKA, Shin-ichi; KAMADA, Masao; IKENAGA, Eiji[3]; SEKITANI, Tetsuji[3]; TANAKA, Ken-ichiro[3]
([1]Nagoya Univ.; [2]KEK-PF; [3]Hiroshima Univ.)

[*Jpn. J. Appl. Phys.* **39**, 4489 (2000)]

Electron-ion coincidence (EICO) spectroscopy [K. Mase, M. Nagasono, S. Tanaka, M. Kamada, T. Urisu and Y. Murata, *Rev. Sci. Instrum.* **68**, 1703 (1997)] has recently been developed to investigate the process of ion desorption induced by the core level excitation. In the present study, we apply EICO spectroscopy to determine the O1s level of condensed H_2O (ice) at 100 K. The kinetic energy of O1s photoelectrons which gives the highest coincidence yield of H^+ desorption is shifted by about –0.7 eV compared to the O1s peak observed in the conventional core-level photoelectron spectroscopy. It is ascribed to a core-level shift in the O1s level from which hydrogen ions desorb. The results indicate the advantages and the possibilities of the EICO spectroscopy for surface analysis.

VI-Q-6 Photo-Stimulated Ion Desorption from TiO_2(110) Surface

TANAKA, Shin-ichiro[1]; MASE, Kazuhiko[2]; NAGAOKA, Shin-ichi; KAMADA, Masao
([1]Nagoya Univ.; [2]KEK-PF)

Photo-stimulated desorption of O^+ from TiO_2(110) surface is investigated by using the electron-photoion coincidence spectroscopy. It is found that O^+ desorbs as a result of the multi-electron excitation/decay of the O1s electron, which can be explained within the expansion of the well-known Knotek-Feibelman mechanism. On the other hand, the Knotek-Feibelman mechanism does not seem to work for the O^+ desorption following the Ti-core excitation. We propose a new model in which the O^+ desorption is induced by the excitation of a Ti-core level: the charge transfer from O2p to Ti3d induced by the Ti3p-core hole potential is responsible for the creation of O^+ ions and its desorption. A discussion on the new model is made for ion desorption from other materials.

VI-Q-7 Ion Desorption Induced by Core-Level Excitation on H_2O/Si(100) Surface

TANAKA, Shin-ichiro[1]; MASE, Kazuhiko[2]; NAGAOKA, Shin-ichi; KAMADA, Masao
([1]Nagoya Univ.; [2]KEK-PF)

Ion desorption from H_2O/Si(100) induced by the O1s-excitation is investigated by the use of the photoelectron, the photon-stimulated desorption and the electron-ion coincidence spectroscopy. It is shown that ion desorption induced by the soft-X-ray is mainly caused by shake-up/off excitation accompanied with the core-excitation and with the Auger decay that results in the multi-holes final state. The core-excitation to the anti-bonding orbital or normal Auger decay that creates the two-holes final state is less important.

VI-Q-8 Resonant Auger Spectrum Following Kr:2p → 5s Photoexcitation

NAGAOKA, Shin-ichi; IBUKI, Toshio[1]; SAITO, Norio[2]; SHIMIZU, Yuichiro; SENBA, Yasunori[3]; KAMIMORI, Katsura[3]; TAMENORI, Yusuke[4]; OHASHI, Haruhiko[4]; SUZUKI, Isao H.[2]
([1]Kyoto Univ. Edu.; [2]Electrotechnical Lab.; [3]Hiroshima Univ.; [4]JASRI)

[*J. Phys. B: At. Mol. Opt. Phys.* **33**, L605 (2000)]

Resonant Auger electron spectra following Kr:2p → 5s photoexcitation have been measured for the first time using monochromatized undulator radiation and a cylindrical-mirror electron-energy analyzer. It is found that the kinetic energy of the resonant Auger electron is higher than that of the corresponding normal Auger electron. The angular distribution of the resonant Auger electrons is nearly isotropic relative to the polarization direction of the incident light.

VI-Q-9 Molecular Deformation in the O $1s^{-1}2\pi_u$ Excited States of CO_2 Probed by the Triple-Differential Measurement of Fragment Ions

SAITO, Norio[1]; UEDA, Kiyoshi[2]; SIMON, Marc[3]; OKADA, Kazumasa[4]; SHIMIZU, Yuichiro; CHIBA, Hisashi[2]; SENBA, Yasunori[4]; OKUMURA, Hiroki[5]; OHASHI, Haruhiko[6]; TAMENORI, Yusuke[6]; NAGAOKA, Shin-ichi; HIRAYA, Atsunari[4]; YOSHIDA, Hiroaki[4]; ISHIGURO, Eiji[7]; IBUKI, Toshio[8]; SUZUKI, Isao H.[1]; KOYANO, Inosuke[5]
([1]Electrotechnical Lab.; [2]Tohoku Univ.; [3]LURE; [4]Hiroshima Univ.; [5]Himeji Inst. Tech.; [6]JASRI; [7]Univ. Ryukyus; [8]Kyoto Univ. Educ.)

[*Phys. Rev. A* **62**, 042503 (2000)]

Measurement of mass-, energy- and angle-resolved

fragment ions revealed that the β value for C^+ with kinetic energy ≥ 3 eV is ~0.9 in the region of the O 1*s* → $2\pi_u$ excitation and that β value for O^+ with kinetic energy ≥ 4 eV varies from –0.23 to –0.57 across the O 1*s* → $2\pi_u$ resonance. These findings postulate that the CO_2 molecule excited to the lower branch of the vibronically split O $1s^{-1}2\pi_u$ excited states deforms into a bent geometry while the molecule excited to the higher branch remains in a linear geometry.

VI-Q-10 Monochromator for a Soft X-ray Photochemistry Beamline BL27SU of SPring-8

OHASHI, Haruhiko[1]; ISHIGURO, Eiji[2]; TAMENORI, Yusuke[1]; OKUMURA, Hiroki[3]; HIRAYA, Atsunari[4]; YOSHIDA, Hiroaki[4]; SENBA, Yasunori[4]; OKADA, Kazumasa[4]; SAITO, Norio[5]; SUZUKI, Isao H.[5]; UEDA, Kiyoshi[6]; IBUKI, Toshio[7]; NAGAOKA, Shin-ichi; KOYANO, Inosuke[3]; ISHIKAWA, Tetsuya[1]
([1]JASRI; [2]Univ. Ryukyus; [3]Himeji Inst. Tech.; [4]Hiroshima Univ.; [5]Electrotechnical Lab.; [6]Tohoku Univ.; [7]Kyoto Univ. Edu.)

[*Nucl. Instrum. Methods Phys. Res., Sect. A* **467–468**, 533 (2001)]

A high-resolution monochromator with varied line space plane gratings (VLSG) and spherical focusing mirrors was installed in one of three branches of BL27SU in SPring-8. The performance of the monochromator was roughly evaluated from the photo ion yield of nitrogen molecule. Furthermore, the kinetic energy of the photoelectron from Xe $5p_{3/2}$ orbital was also measured at the same photon energy with the N_2 to avoid the influence of natural width. The resolving power over 10^4 has been confirmed at the N K-edge.

VI-Q-11 Angle-Resolved Electron and Ion Spectroscopy Apparatus on the Soft X-Ray Photochemistry Beamline BL27SU at SPring-8

UEDA, Kiyoshi[1]; YOSHIDA, Hiroaki[2]; SENBA, Yasunori[2]; OKADA, Kazumasa[2]; SHIMIZU, Yuichiro; CHIBA, Hisashi[1]; OHASHI, Haruhiko[3]; TAMENORI, Yusuke[3]; OKUMURA, Hiroki[4]; SAITO, Norio[5]; NAGAOKA, Shin-ichi; HIRAYA, Atsunari[2]; ISHIGURO, Eiji[6]; IBUKI, Toshio[7]; SUZUKI, Isao H.[5]; KOYANO, Inosuke[4]
([1]Tohoku Univ.; [2]Hiroshima Univ.; [3]JASRI; [4]Himeji Inst. Tech.; [5]Electrotechnical Lab.; [6]Univ. Ryukyus; [7]Kyoto Univ. Edu.)

[*Nucl. Instrum. Methods Phys. Res., Sect. A* **467–468**, 1502 (2001)]

We have designed and constructed the apparatus for the angular distribution measurements of photoejected electrons and ions from free molecules, as a part of the endstation of a *c*-branch of the beamline BL27SU, a soft X-ray photochemistry beamline at SPring-8. The experimental procedures are described in combination with the use of a capability to switch the horizontal and vertical directions of the linear polarization of the light produced by the figure-8 undulator. As a typical example of the experimental results, we present angle-resolved energetic ion yield spectra in the O 1s excitation region of CO_2.

VI-Q-12 Resonant Auger Spectra of Kr Near the L_3 Threshold

IBUKI, Toshio[1]; OKADA, Kazumasa[2]; KAMIMORI, Katsura[2]; SASAKI, Junko[2]; YOSHIDA, Hiroaki[2]; HIRAYA, Atsunari[2]; SUZUKI, Isao H.[3]; SAITO, Norio[3]; NAGAOKA, Shin-ichi; SHIMIZU, Yuichiro; OHASHI, Haruhiko[4]; TAMENORI, Yusuke[4]
([1]Kyoto Univ. Edu.; [2]Hiroshima Univ.; [3]Electrotechnical Lab.; [4]JASRI)

Auger electron spectra were studied by scanning the photon energy near the L_3 threshold of krypton. Two resonant transitions were observed in the photon energy region 1673–1678 eV for the first time. They were identified to be the resonant $3d^{-2}5s$ and $3d^{-2}4d$ states originating from the $2p_{3/2}{}^{-1}5s$ and $2p_{3/2}{}^{-1}4d$ excitations, respectively.

VI-Q-13 Auger Electron Spectra of Kr2p Holes Using Monochromatic Soft X-Rays

SUZUKI, Isao H.[1]; OKADA, Kazumasa[2]; KAMIMORI, Katsura[2]; SASAKI, Junko[2]; YOSHIDA, Hiroaki[2]; HIRAYA, Atsunari[2]; SHIMIZU, Yuichiro; NAGAOKA, Shin-ichi; TAMENORI, Yusuke[3]; OHASHI, Haruhiko[3]; IBUKI, Toshio[4]
([1]Electrotechnical Lab.; [2]Hiroshima Univ.; [3]JASRI; [4]Kyoto Univ. Edu.)

Normal Auger electron spectra from Kr2p hole states, $L_{23}M_{45}M_{45}$ and $L_{23}M_{23}M_{45}$, have been measured using monochromatized synchrotron radiation and a high resolution electron spectrometer. Measured spectra were reproduced with a fitting calculation, where Voigt functions including an instrumental resolution and natural lifetime widths of related core hole states were used. At most final states estimated energies for spectral peaks agree with those by electron and ion beam techniques. Relative intensities for some peaks are appreciably different from the previous results.

VI-R Ultraviolet Photoelectron Spectroscopy of Organic Thin Film and Organic/Inorganic Interface

Electronic structures of organic film surface and organic/inorganic interface are expected to play an important role in organic-device properties. We investigated surface structures and energy alignments to clarify their electronic structures using electron spectroscopy such as photoelectron spectroscopy combined with synchrotron radiation and metastable atom electron spectroscopy.

VI-R-1 Pendant Group Orientation of Poly(2-vinylnaphthalene) Thin Film Surface Studied by Near-Edge X-Ray Absorption Fine Structure Spectroscopy (NEXAFS) and Angle-resolved Ultraviolet Photoelectron Spectroscopy (ARUPS)

MORIKAWA, Eizi[1]; SAILE, Volker[1]; OKUDAIRA K., Koji; AZUMA, Yasushi[2]; MEGURO, Kazuyuki[2]; HARADA, Yoshiya[2]; SEKI, Kazuhiko[3]; HASEGAWA, Shinji; UENO, Nobuo[2]
([1]Louisiana State Univ. CAMD; [2]Chiba Univ.; [3]Nagoya Univ.)

[*J. Chem. Phys.* **112**, 10476 (2000)]

Angle-resolved ultraviolet photoelectron spectroscopy (ARUPS) and near-edge x-ray absorption fine structure (NEXAFS) spectroscopy were applied to the investigation of the tilt angles of the naphthalene pendant groups at the surface of poly(2-vinyl-naphthalene) thin film. The NEXAFS results indicates that the mean value of tilt angle of naphthalene pendant groups with respect to the polymer surface is about 57°. In contrast to NEXAFS, which provides only an average determination of the tilt angle, ARUPS combined with a sophisticated analysis of photoelectron angular dependence offers more detailed information. Analysis by ARUPS combined with the single-scattering approximation with molecular orbital calculation indicates that the naphthalene pendant groups are tilted randomly at the polymer surface, and that the tilt angle distribution is well described as a three-dimensional isotropic random orientation, which indicates that the majority of the pendant groups is tilted at large angles with respect to the polymer surface.

VI-R-2 Origin of Indium-[perylene3,4,9,10-tetracarboxylic Dianhydride] Interface States Studied by Outermost Surface Spectroscopy Using Metastable Atoms

KERA, Satoshi[1]; SETOYAMA, Hiroyuki[1]; OKUDAIRA K., Koji; HARADA, Yoshiya[2]; UENO, Nobuo[1]
([1]Chiba Univ.; [2]Seitoku Univ.)

[*Phys. Rev. B* **63**, 115204 (2001)]

Metastable atom electron spectra (MAES) and ultraviolet photoelectron spectra (UPS) of indium-[perylene3,4,9,10-tetracarboxylic dianhydride (PTCDA)] system prepared on a MoS_2 single crystal substrate were measured as a function of the In over-layer thickness (ΘIn). As observed by a previous UPS experiment, a new band was observed in the original PTCDA energy gap region even by the MAES which detects the outermost surface selectively (Figure 1). The ΘIn dependence of this new band intensity measured by the MAES gives a maximum at ΘIn ~ 1 Å, suggesting that four In atoms are reacting with one PTCDA molecule at the C=O parts. From the result of the density functional theory (DFT) methods and the enhanced intensity of the new band in the MAES, it was concluded that the new band originates from π state consisting of In 5pz AO's.

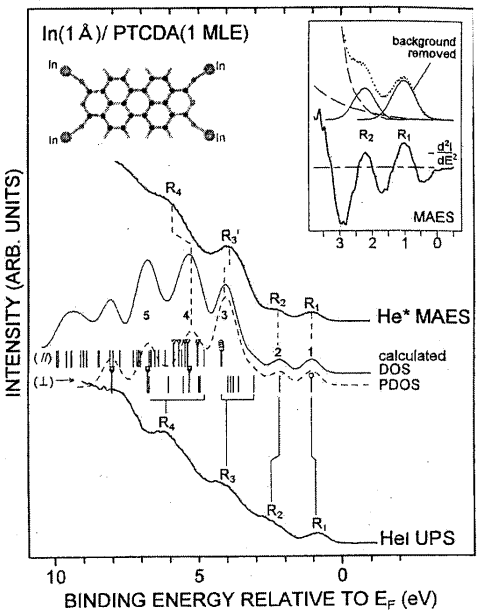

Figure 1. Comparison of the observed He*(2^3S) MAES and He I UPS of the In(1 Å)/PTCDA(1 MLE)/MoS_2 and the calculated results for In_4PTCDA. Bars show calculated MO energy levels obtained by DFT method (B3LYP/LanL2DZ). The Upper and lower bars respectively, indicate $MO_{//}$ and $MO_{\perp}$ states, and bars with circles show states with large contribution of In AO's (5p,5s). Bars with triangles indicate states with contribution of oxygen AO's. The calculated DOS is shown by solid curve. The PDOS, which corresponds to partial DOS for $MO_{\perp}$ and four contracted σ states (marked by circles in $MO_{//}$), is shown by a dashed curve. These DOS's were observed by 0.7 eV Gaussian broadening of MO's. Negative of the second derivative of the MAES ($-d^2I/dE^2$) and the MAES after background removal is shown in inset, in order to show the enhanced intensity of band R_1 than band R_2. Molecular structure of the reaction product, In_4PTCDA, is also shown.

VI-R-3 Surface Images of SiO_2/Si(100) Pattern using Electron Emission Microscopy with Metastable Atoms, Photons and Low-Energy Electrons

YASUFUKU, Hideyuki[1]; OKUMURA, Masao[1]; IBE, Takehiro[1]; OKUDAIRA K., Koji; HARADA, Yoshiya[2]; UENO, Nobuo[1]
([1]Chiba Univ.; [2]Seitoku Univ.)

[*Jpn. J. Appl. Phys.* **40**, 2447 (2001)]

The surface images of a SiO_2 pattern on Si(100) was observed by three types of electron emission microscopies, *i.e.*, metastable electron emission microscopy (MEEM) with metastable he, photoelectron emission microscopy (PEEM) and low-energy electron emission microscopy (LEEM). Among these, MEEM gave the most diffused image at the pattern edges of the SiO_2 region. Furthermore, it is found that the difference in MEEM, LEEM, and PEEM images can provide new information on the spatial distribution of surface electronic state. By comparing MEEM, LEEM, and PEEM images, it is expected that we can obtain local information on surface electronic states in more detail

VI-R-4 Ultraviolet Photoelectron Spectra of Metallofullerenes, Two Ca@C_{82} Isomers

HINO, Shojun[1]; UMISHITA, Kazunori[1]; IWASAKI, Kentaro[1]; AOKI, Masaru; KOBAYASHI, Kaoru[2]; NAGASE, Shigeru[2]; DENNIS, T. John S.[3]; NAKANE, Tomoyasu[3]; SHINOHARA, Hisanori[3]
([1]Chiba Univ.; [2]Tokyo Metro. Univ.; [3]Nagoya Univ.)

[*Chem. Phys. Lett.* **337**, 65 (2001)]

Ultraviolet photoelectron spectra (UPS) of two Ca@C_{82} isomers (III and IV) were measured with a synchrotron radiation light source. Figure 1 shows these photoelectron spectra obtained with 20 eV excitation energy. The photoelectron onset energies of isomer III and IV were 0.7 eV and 0.8 eV below the Fermi level, respectively, which indicates their semiconductive nature. When the excitation energy is tuned, spectral intensity changes as other fullerenes have shown. Their upper valence band (0–5 eV) spectra are different from those of other metallofullerenes such as La@C_{82}, Sc@C_{82} and Gd@C_{82} as well as those of empty C_{82} but their lower valence band spectra (below 5 eV) are almost identical. Comparison between the UPS and *ab initio* calculation assuming transfer of two electrons from encapsulated calcium atom to the cage (*i.e.* $Ca^{+2}@C_{82}^{2-}$) suggests C_2(c) geometry for isomer III and C_s for isomer IV.

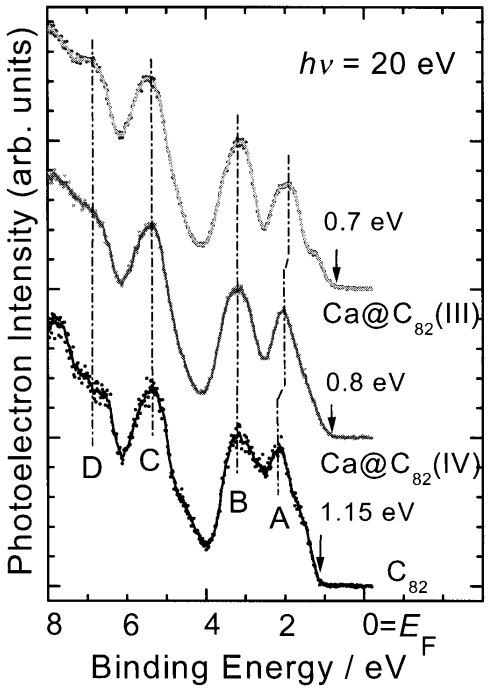

Figure 1. UPS spectra of two Ca@C_{82} isomers and C_{82}.

VI-R-5 Chemical Reaction at the NTCDA/Metal Interfaces

MARUYAMA, Takahiro[1]; SUGAWARA, Norikazu[2]; HIRASAWA, Akira[2]; AKIMOTO, Katsuhiro[2]
([1]Ritsumeikan Univ.; [2]Inst. Appl. Phys., Univ. Tsukuba)

Planar π-stacking organic molecules have been shown to be excellent model compounds for studying the growth and optoelectronic properties of organic semiconducting thin films on metal substrates.[1)] In this study, we investigated the bonding of 1,4,5,8-naphthalene-tetracaboxylicacid-dianhydride (NTCDA) on Au and In by ultra-violet photoemission spectroscopy (UPS). Figures 1 and 2 show the valence band of NTCDA on Au and In, respectively, as a function of the amount of NTCDA deposition. The structures due to the highest occupied molecular orbital (HOMO) of NTCDA are seen even at low coverage on Au. However, the spectra of NTCDA deposited on Al are quite different from those on Au even at 50 Å. Taking into account the results of AES measurements, it is considered that NTCDA molecules are weakly bonded to Au substrate through the HOMO, on the other hand, a strong chemical bond between In and the anhydride group of NTCDA is formed and results in the diffusion of In atoms into NTCDA films.

Reference

1) Y. Hirose, A. Kahn, V. Aristov, P. Soukiassian, V. Bulovic and S. R. Forrest, *Phys. Rev. B* **54**, 13748 (1996).

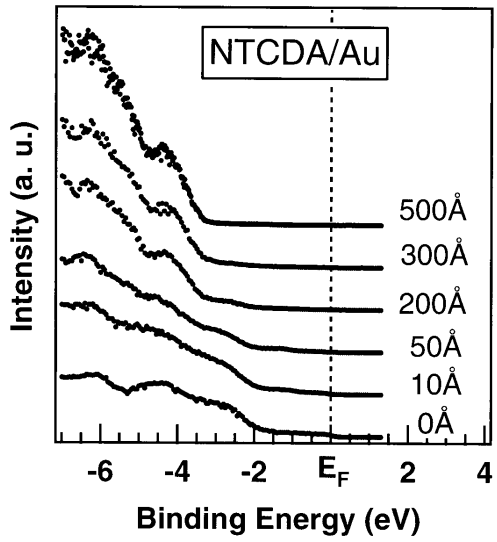

Figure 1. Valence band UPS spectra for NTCDA on Au.

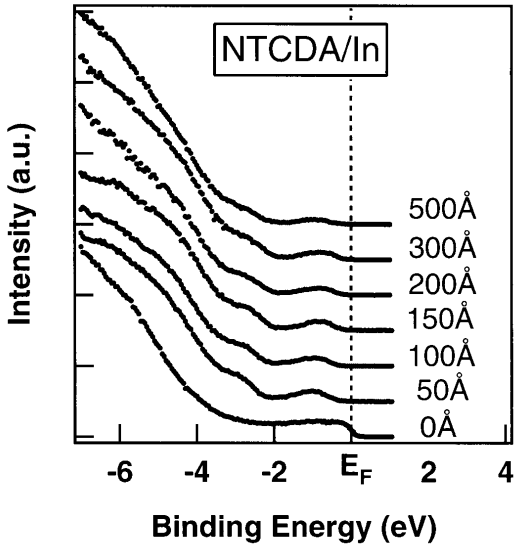

Figure 2. Valence band UPS spectra for NTCDA on In.

VI-S Study on Compact X-Ray Sources

Electron storage rings are useful and practical devices as x-ray sources because which produce a number of photons because of high electron current and various insertion devices. However, these synchrotron radiation facilities usually occupy large area and cost much. So that there have been many works to investigate compact x-ray sources such as x-ray lasers and free electron lasers. It is also useful to use laser undulator radiation or backward Compton scattering caused by the interactions of electron beams with laser photons, if we provide enough electrons to produce practical intensity of x-rays. RF-photocathode would produce dense electron beam so that it is a useful candidate of a electron source. It is necessary to search good materials as the photocathode for construction of a practical compact x-ray source. Cesium telluride has reported to have a good quantum efficiency, so that we have studied about it.

X-ray sources must be shielded for radiation safety. For constructing effective shields, we need to know how many radiations are yielded from our x-ray sources. We will use high energy electrons to produce x-rays and loss of the electrons cause radiations, it is useful to study radiations in synchrotron radiation facilities in order to estimate the yields radiations from our x-ray sources. We preliminarily measured radiations radiated from a vacuum duct of UVSOR.

VI-S-1 Preliminary Study on Photoemission from Cesium Telluride Irradiated by Polarized Photon

TAKASHIMA, Yoshifumi; KOBAYAKAWA, Hisashi[1]; TAKAGI, Masahiro[1]; KIMURA, Kenichi[1]; SUGIYAMA, Harue[1]; FURUTA, Fumio[1]; NAKANISHI, Tsutomu[1]
([1]Nagoya Univ.)

Cesium telluride is a good candidate for a material to be used as a photocathode for RF-gun because of its high quantum efficiency and long life. The quantum efficiency of the photocathode for polarized photon measured with changing the incident angle of the light gives us important information about the optical constants of the materials of the photocathode.

We measured the quantum efficiency of cesium telluride by using linear polarized photon. Figure 1 shows a sketch of our experimental set up. A Xe lamp was used as a light source. The light from the Xe lamp passed through a monochrometer and a polarizer enter a vacuum chamber in which cesium telluride was evaporated on molybdenum block as a photocathode. The incident angle of the light was changed from –80° to 80°. We rotated the polarizer in order to change the direction of polarization. Figure 2 shows the quantum efficiency for the incident light of 250 nm wavelength. Closed and open circles show the quantum efficiency for the light which is polarized parallel (p-polarization) and perpendicular (s-polarization) to the incident plane, respectively. The quantum efficiency of p-polarization light has peaks at ±65°.

We assume that the quantum efficiency is proportional to (1-R) in order to calculate the optical constants of the photocathode of cesium telluride by using Fresnel formulas. R is reflectivity of the incident light from the photocathode. We obtain preliminary results of optical constants of cesium telluride. The refractive index and the extinction coefficient are 3.17 and 1.01 respectively.

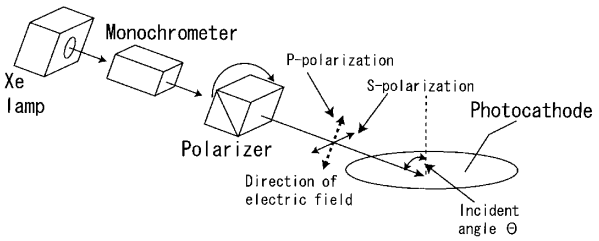

Figure 1. Sketch of experimental set up.

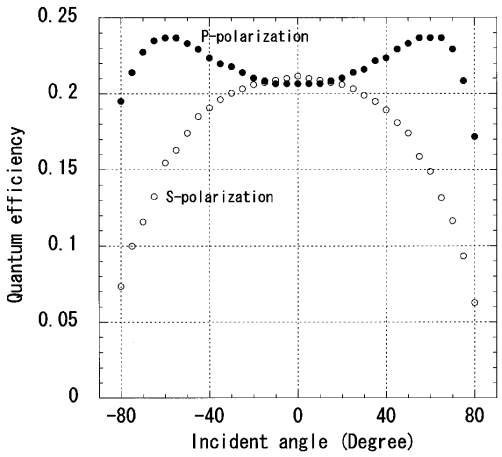

Figure 2. Quantum efficiency of cesium telluride with incident angle of light. The wavelength of the light is 250 nm. Open and closed circles show the quantum efficiency for the incident light which is polarized parallel and perpendicular to the incident plane, respectively.

VI-S-2 Study on Radiation Shielding for Synchrotron Radiation Facilities

TAKASHIMA, Yoshifumi; KOBAYAKAWA, Hisashi[1]; OKI, Sota[1]; YAMAKAGE, Masahiro[1]; TOMIHIRA, Kiyotaka[1]
([1]Nagoya Univ.)

Radiation shielding for synchrotron facilities is to be effective in protecting radiations. In order to design effective shields, we need to estimate how many radiations are generated from a storage ring and

penetrate radiation shields.

Electron loss in beam ducts cause considerable stray radiations. Circulating electrons in a storage ring go out of their stable orbit if they interact with residual gases or other electrons. Electrons are also lose when they radiate high energy synchrotron radiations. These electrons are incident on the beam duct and generate electromagnetic showers around the ring.

We measured energy depositions of electromagnetic shower in NaI(Tl) scintillation counter generated by beam loss in a beam duct of UVSOR storage ring. Figure 1 shows experimental setup schematically. The diameter and thickness of the NaI(Tl) are 1 inch and 2 mm, respectively. The detection angles were 40° and 60°. Figure 2 shows pulse height distributions of energy depositions in NaI(Tl) for each detection angles. The energy deposition at 40° is larger than 60° because the incident angle of electrons in the beam duct is smaller than 40° and electromagnetic showers grow toward the incident angle.

For further study, we should measure the energy deposition in NaI(Tl) counter at smaller detection angles than 40° in order to estimate the incident angle of electrons in the beam duct. The information of the incident angle is important to calculate the spatial distribution of the dose around a storage ring. We should also investigate the absolute intensity of electromagnetic shower by comparing experimental results and theoretical calculations in order to estimate yields of radiations precisely for facilities of compact x-ray sources.

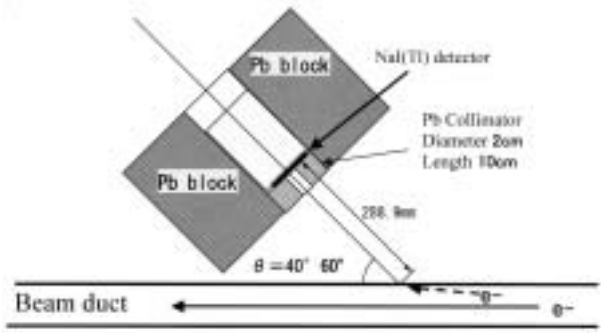

Figure 1. Experimental setup.

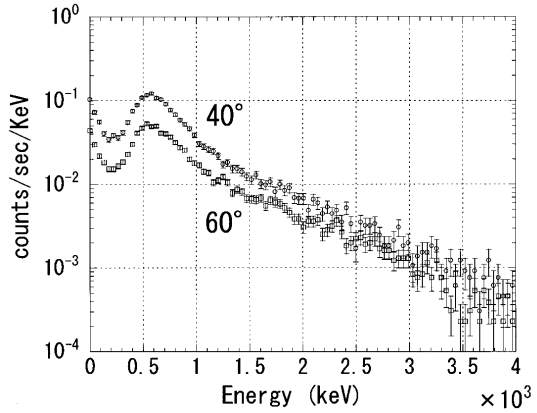

Figure 2. Pulse height distribution of energy deposition in NaI(Tl) detector. Open circles and open squares show the experimental data for detection angle of 40° and 60°, respectively.

VI-T Syntheses of Fullerene-Based New Materials with Novel Physical Properties

Fullerene-based new materials are synthesized, and the structures and physical properties are studied in wide temperature and pressure regions. The structures and transport properties of pressure-induced superconducting fulleride, Cs_3C_{60}, are studied by X-ray powder diffraction, ESR, Raman, AC susceptibility and resistivity measurements, in order to clarify the mechanism of pressure-induced superconductivity. The two-dimensional polymeric fulleride, Na_4C_{60}, is also studied in order to clarify the novel physical properties which are expected from its low-dimenionality. The structures and electronic properties of solid metallofullerenes are first clarified under high pressure, and the first evidence has been obtained for the endohedral structure and electron transfer from a metal atom to the C_{60} cage in metal endohedral C_{60}.

VI-T-1 Structure and Raman Scattering of Cs_3C_{60} under High Pressure

FUJIKI, Satoshi; KUBOZONO, Yoshihiro; EMURA, Shuichi[1]; TAKABAYASHI, Yasuhiro; KASHINO, Setsuo[2]; FUJIWARA, Akihiko[3]; ISHI, Kenji[3]; SUEMATSU, Hiroyoshi[3]; MURAKAMI, Yoichi[4]; IWASA, Yoshihiro[5]; MITANI, Tatsuoki[5]; OGATA, Hironori
([1]Osaka Univ.; [2]Okayama Univ.; [3]Univ. Tokyo; [4]KEK-PF; [5]JAIST)

[*Phys. Rev. B* **62**, 5366 (2000)]

Raman scattering is studied for a pressure-induced superconductor Cs_3C_{60} in a pressure region from 1 bar to 62 kbar. The center frequency ω_0 for $H_g(1)$ and $H_g(2)$ Raman peaks increases by applying pressure, but the increase shows a saturation in the high-pressure region. On the other hand, the ω_0 for $A_g(1)$ and $A_g(2)$ modes increase monotonically in all pressure regions. The electron-phonon coupling constant for Cs_3C_{60} shows a rapid decrease up to 30 kbar and an increase above 30 kbar. This result may be associated with a transformation from a multiphase (body-centered orthorhombic and A15 phases) to a single phase around 20 kbar. X-ray powder diffraction pattern at 11 K under a pressure of 40 kbar shows that a superconducting phase for Cs_3C_{60} is body-centered orthorhombic.

VI-T-2 Structure and Physical Properties of Na_4C_{60} under Ambient and High Pressures

KUBOZONO, Yoshihiro; TAKABAYASHI, Yasuhiro; KAMBE, Takashi[1]; FUJIKI, Satoshi; KASHINO, Setsuo[1]; EMURA, Shuichi[2]
([1]Okayama Univ.; [2]Osaka Univ.)

[*Phys. Rev. B* **63**, 45418 (2001)]

The structure and physical properties of two-dimensional polymeric Na_4C_{60} (body-centered monoclinic, space group *I*2/*m*) are studied in a wide temperature region from 12 to 300 K at 1 bar, and in a pressure region up to 53 kbar at 300 K. The temperature dependence of lattice constants suggests a structural anomaly below 100 K where the variation of spin susceptibility is observed from electron spin resonance. The thermal expansion of the unit-cell volume V is smaller than that of monomeric Rb_3C_{60} and K_3C_{60}. The compressibility of *c* is larger than that of *a* and *b*, which can be well explained by the repulsion between Na ions. The compressibility of the center-to-center distance in the $(10\bar{1})$ plane is ~ 1/3 times smaller than that in the (101) plane, which can be well explained by the formation of the polymer chains. Further, a possibility of a three-dimensional polymerization is discussed on the basis of the pressure dependence of $C_{60}\cdots C_{60}$ distance.

VI-T-3 Structure of $La_2@C_{80}$ Studied by La K-Edge XAFS

KUBOZONO, Yoshihiro; TAKABAYASHI, Yasuhiro; KASHINO, Setsuo[1]; KONDO, Masahiro[2]; WAKAHARA, Takatsugu[2]; AKASAKA, Takeshi[3]; KOBAYASHI, Kaoru[4]; NAGASE, Shigeru; EMURA, Shuichi[5]; YAMAMOTO, Kazunori[6]
([1]Okayama Univ.; [2]Niigata Univ.; [3]Univ. Tsukuba; [4]Tokyo Metropolitan Univ.; [5]Osaka Univ.; [6]Power Reactor and Nuclear Fuel Department Corporation)

[*Chem. Phys. Lett.* **335**, 163 (2001)]

The structure of $La_2@C_{80}$ is studied by La K-edge XAFS from 40 to 295 K. The distances between the La atom and the first nearest C atoms have been determined to be 2.42(1) Å at 40 K and 2.44(2) Å at 295 K, and those between the La atom and the second nearest C atoms to be 2.97(2) Å at 40 K and 2.98(3) Å at 295 K. The La–La distance has been determined to be 3.90(1) Å at 40 K and 3.88(2) Å at 295 K. The temperature dependence of the mean-square displacement of La–C is also studied to get an insight into the dynamical behavior of two La atoms in the C_{80} cage.

VI-T-4 Structure and Electronic Properties of $Dy@C_{82}$ Studied by UV-VIS Absorption, X-Ray Powder Diffraction and XAFS

IIDA, Satoru[1]; KUBOZONO, Yoshihiro; SLOVOKHOTOV, Yuri[2]; TAKABAYASHI, Yasuhiro; KANBARA, Takayoshi; FUKUNAGA, Takeo[1]; FUJIKI, Satoshi; EMURA, Shuichi[3]; KASHINO, Setsuo[1]
([1]Okayama Univ.; [2]Russian Acad. Sci.; [3]Osaka Univ.)

[*Chem. Phys. Lett.* **338**, 21 (2001)]

Two isomers of Dy@C_{82} were separated by high performance liquid chromatography (HPLC), and their UV-VIS absorption spectra were measured to characterize these isomers. The crystalline powder of Dy@C_{82} was obtained by removing solvent (toluene) at 250 °C under vacuum. The X-ray diffraction pattern can be indexed with fcc crystal lattice, as that in La@C_{82}. The lattice constant *a* at 298 K, 15.86(1) Å, is close to that of La@C_{82}, 15.78 Å. The distances between Dy and the first and second nearest C atoms are determined to be 2.52(2) and 2.86(2) Å, respectively, on the basis of Dy L_{III}-edge EXAFS. The XANES shows that the valence of the Dy atom in Dy@C_{82} is +3.

VI-T-5 Dy@C_{60}: Evidence for Endohedral Structure and Electron Transfer

KANBARA, Takayoshi; KUBOZONO, Yoshihiro; TAKABAYASHI, Yasuhiro; FUJIKI, Satoshi; IIDA, Satoru[1]; HARUYAMA, Yusuke[1]; KASHINO, Setsuo[1]; EMURA, Shuichi[2]; AKASAKA, Takeshi[3]
([1]Okayama Univ.; [2]Osaka Univ.; [3]Univ. Tsukuba)

[*Phys. Rev. B* **64**, 113403 (2001)]

In view of the lack of information on the structure of M@C_{60} (M: alkaline earth and lanthanide metal) because of its instability and difficulties in purifying it, we have carried out and report here some structural investigations of Dy@C_{60}. We obtained a pure sample of Dy@C_{60} by high performance liquid chromatography with aniline as an eluent, and studied it by Dy L_{III}-edge XAFS and Raman scattering. Our results show conclusively that the structure is endohedral (with the metal inside the C_{60} cage) and that electron transfer takes place between Dy and C_{60}. The Dy in Dy@C_{60} is located at an off-center position, 1.25–1.30 Å, from the center of the C_{60} cage. The valence of the Dy is shown to be + 3 on the basis of a Dy L_{III}-edge XANES study. The $A_g(2)$ Raman peak also shows that three electrons have been transferred from Dy atom to the C_{60} cage. The UV-VIS-IR spectrum suggests that the HOMO-LUMO gap is small.